CDYL2 Epigenetically Regulates MIR124 to Control NF-kB/STAT3-Dependent Breast Cancer Cell Plasticity

Maha Siouda, Audrey D Dujardin, Laetitia Barbollat-Boutrand, Marco Mendoza-Parra, Benjamin Gibert, Maria Ouzounova, Jebrane Bouaoud, Laurie Tonon, Marie Robert, Jean-Philippe Foy, et al.

iScience

CellPress
OPEN ACCESS

Article

CDYL2 Epigenetically Regulates *MIR124* to Control NF-κB/STAT3-Dependent Breast Cancer Cell Plasticity

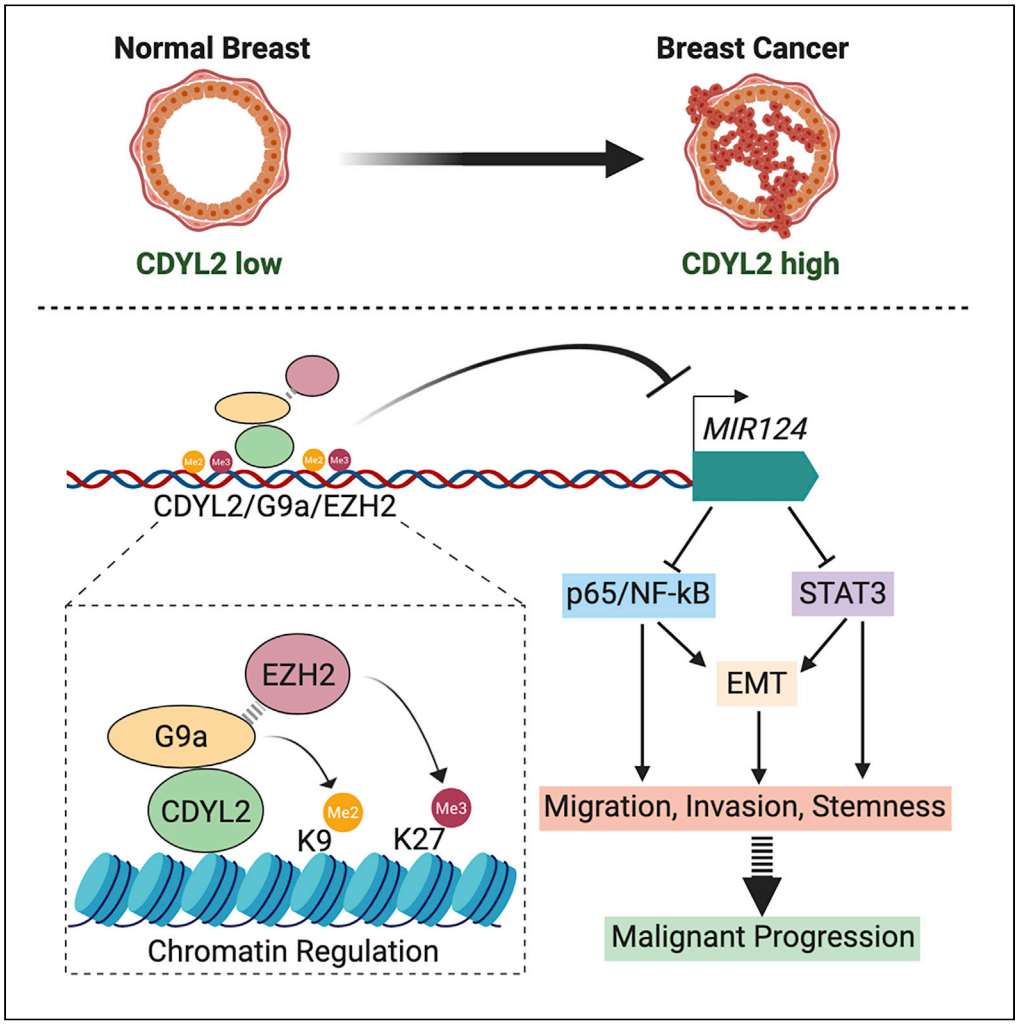

Maha Siouda, Audrey D. Dujardin, Laetitia Barbollat-Boutrand, ..., Hinrich Gronemeyer, Pierre Saintigny, Peter Mulligan

peter.mulligan@inserm.fr

HIGHLIGHTS

Up-regulation of CDYL2 is common in breast cancer and correlates with poor prognosis

CDYL2 regulates enrichment of methyltransferases G9a and EZH2 at *MIR124* genes

microRNA-124 regulation by CDYL2 impacts STAT3 and NF-κB signaling

CDYL2 regulation of EMT, migration, invasion, and stemness is STAT3/NF-κB dependent

Siouda et al., iScience *23*, 101141
June 26, 2020
https://doi.org/10.1016/j.isci.2020.101141

iScience

CellPress
OPEN ACCESS

Article

CDYL2 Epigenetically Regulates *MIR124* to Control NF-κB/STAT3-Dependent Breast Cancer Cell Plasticity

Maha Siouda,[1] Audrey D. Dujardin,[1] Laetitia Barbollat-Boutrand,[1] Marco A. Mendoza-Parra,[2,8] Benjamin Gibert,[1] Maria Ouzounova,[1,3] Jebrane Bouaoud,[1,4] Laurie Tonon,[5,6] Marie Robert,[1,3] Jean-Philippe Foy,[1,3] Vincent Lavergne,[1,3] Serge N. Manie,[1] Alain Viari,[5,6] Alain Puisieux,[1,3] Gabriel Ichim,[1] Hinrich Gronemeyer,[2] Pierre Saintigny,[1,3] and Peter Mulligan[1,7,9,*]

SUMMARY

Epigenetic deregulation of gene transcription is central to cancer cell plasticity and malignant progression but remains poorly understood. We found that the uncharacterized epigenetic factor chromodomain on Y-like 2 (CDYL2) is commonly over-expressed in breast cancer, and that high CDYL2 levels correlate with poor prognosis. Supporting a functional role for CDYL2 in malignancy, it positively regulated breast cancer cell migration, invasion, stem-like phenotypes, and epithelial-to-mesenchymal transition. CDYL2 regulation of these plasticity-associated processes depended on signaling via p65/NF-κB and STAT3. This, in turn, was downstream of CDYL2 regulation of *MIR124* gene transcription. CDYL2 co-immunoprecipitated with G9a/EHMT2 and GLP/EHMT1 and regulated the chromatin enrichment of G9a and EZH2 at *MIR124* genes. We propose that CDYL2 contributes to poor prognosis in breast cancer by recruiting G9a and EZH2 to epigenetically repress *MIR124* genes, thereby promoting NF-κB and STAT3 signaling, as well as downstream cancer cell plasticity and malignant progression.

INTRODUCTION

A key feature of epigenetic processes is their ability to establish and maintain the expression level of genes in a manner that is durable, yet can be altered when necessary. To this end, the deposition of histone lysine methylation marks on chromatin is tightly regulated. However, deregulation of epigenetic factors can cause pathologic changes in cell identity and function and is a near-universal feature of cancer cells. Such perturbations offer therapeutic opportunities, and several drugs targeting epigenetic regulators are in use or under investigation as cancer treatments. These include inhibitors of the histone methyltransferases EZH2 and G9a, which respectively impart the H3K27me3 and H3K9me2 marks on chromatin (Dawson and Kouzarides, 2012; Jambhekar et al., 2019; Simó-Riudalbas and Esteller, 2015). However, despite recent progress, the epigenetic regulation of cellular plasticity in cancer remains poorly understood, with several putative epigenetic factors still uncharacterized. Addressing these issues could uncover new epigenetic drug targets for cancer treatment.

Most tumors are of epithelial origin, but epithelial cells are inherently resistant to several key steps in malignant progression. Molecular and cellular changes that render carcinoma cells more mesenchymal-like are associated with increased propensity to migrate and invade the surrounding tissues (Puisieux et al., 2014; Shibue and Weinberg, 2017). This so-called epithelial-to-mesenchymal transition (EMT) is also linked to the emergence of cancer stem cells (CSC), a subset of cells within a tumor mass that are highly efficient at seeding new tumor growth and in the case of breast cancer, more efficient at forming cellular aggregates called mammospheres *in vitro* (Shibue and Weinberg, 2017). In breast cancer, different tumor subtypes and prognosis correlate with distinct EMT states. Tumors expressing the estrogen receptor alpha (ER), but not the human epidermal growth factor (EGF) receptor 2 (HER2), are more epithelial-like, less invasive, and have better prognosis, whereas those triple-negative (TN) for expression of ER, HER2, and the progesterone receptor (PR) are more mesenchymal-like, invasive, and have worse prognosis (Sarrio et al., 2008).

[1]Université de Lyon, Université Claude Bernard Lyon 1, INSERM 1052, CNRS 5286, Centre Léon Bérard, Cancer Research Center of Lyon, Lyon, France

[2]Institut de Génétique et de Biologie Moléculaire et Cellulaire (IGBMC), CNRS UMR 7104, INSERM U964, University of Strasbourg, Illkirch, France

[3]Equipe Labellisée Ligue Contre le Cancer, LabEx DEVweCAN

[4]Department of Maxillo-facial Surgery and Stomatology, Pitié-Salpétrière Hospital, Pierre et Marie Curie University Paris 6, Sorbonne Paris Cite University, AP-HP, Paris 75013, France

[5]Synergie Lyon Cancer, Plateforme de Bioinformatique "Gilles Thomas", Centre Léon Bérard, 28 rue Lannec, Lyon 69008, France

[6]INRIA Grenoble-Rhône-Alpes, 655 Avenue de l'Europe, Montbonnot-Saint-Martin 38330, France

[7]Centre de Recherche en Cancérologie de Lyon (CRCL), Centre Léon Bérard, Epigenetics and Cancer Team, Cheney A, 5e étage, 28 rue Laennec, Lyon Cedex 08 69373, France

[8]Present address: Genoscope, CNRS UMR8030, LISSB, SysFate, Evry, France

[9]Lead Contact

*Correspondence: peter.mulligan@inserm.fr

https://doi.org/10.1016/j.isci.2020.101141

However, the acquisition of EMT-like features in a subset of cells within the ER+/HER2- tumor could drive the malignant progression of these cancers.

The gene expression changes underlying EMT and stemness result from interconnected regulatory systems involving transcription factors, epigenetic factors, and non-coding RNAs. In breast cancer, active forms of the transcription factors p65/NF-κB and STAT3 promote EMT, migration, invasion, and stemness (Marotta et al., 2011; Yang et al., 2014; Zhou et al., 2008). Misregulation of EZH2 and G9a can also induce these cellular processes (Chang et al., 2011; Curry et al., 2015; Dong et al., 2012), as can aberrant silencing of the tumor suppressive microRNA-124 (miR-124) (Ji et al., 2019; Lv et al., 2011; Wang et al., 2016a), itself a regulator of p65/NF-κB and STAT3 signaling (Cao et al., 2018; Hatziapostolou et al., 2011; Mehta et al., 2017; Olarerin-George et al., 2013). Recently, EZH2 was implicated in miR-124 repression in renal carcinoma cells (Zhou et al., 2019), supporting an interplay between these pathways. However, by and large, epigenetic regulation of EMT and stemness in cancer remains poorly understood.

In this study, we investigated the molecular and cellular functions of the putative epigenetic factor chromodomain on Y-like 2 (CDYL2) in breast cancer. This is a member of the *CDYL* family of genes, which includes two autosomal homologs in humans, *CDYL1/CDYL* and *CDYL2* (Dorus et al., 2003). The family is defined by the presence of an N-terminal chromodomain that binds to methylated histone H3 lysine 9 (H3K9) and H3K27 residues (Fischle et al., 2008; Franz et al., 2009) and a C-terminal domain homologous to enoyl coenzyme A hydratase/isomerase enzymes (Dorus et al., 2003). *CDYL1* is implicated in cancer as a candidate oncogene or tumor suppressor, depending on the context (Mulligan et al., 2008; Wu et al., 2013), and its epigenetic mechanism involves its interaction with and regulation of several other epigenetic factors, notably the H3K9 methyltransferases G9a/EHMT2, GLP/EHMT1 and SETDB1/ESET (Mulligan et al., 2008), and EZH2 (Zhang et al., 2011). By contrast, very little is known about the roles of *CDYL2* in physiology or disease or its putative epigenetic mechanism.

A potential role for *CDYL2* in cancer was suggested by a genome-wide association study that identified an intronic SNP in *CDYL2* associated with cancer risk (Michailidou et al., 2013). Here we show that CDYL2 expression is also frequently up-regulated in breast cancer, and that high expression correlates with poor outcome in the estrogen receptor-positive/human EGF receptor 2-negative (ER+/HER2−) and TN subtypes. We propose that high levels of CDYL2 expression promote epigenetic repression of *MIR124* genes by increasing G9a and EZH2 recruitment and H3K9 and H3K27 methylation at upstream regulatory regions. This, in turn, contributes to CDYL2 induction of NF-κB and STAT3 signaling, consequent induction of EMT genes, and increased cell motility, invasiveness, and stemness. These findings implicate *CDYL2* as candidate proto-oncogene and therapeutic target in breast cancer.

RESULTS

High CDYL2 Expression Level in Breast Cancer Is Associated with Poor Prognosis

Datamining revealed that CDYL2 mRNA is up-regulated in four breast cancer cohorts within The Cancer Genome Atlas (TCGA) (Cancer Genome Atlas Network, 2012) (Figures 1A and S1A). Similarly, the NCBI GEO datasets GSE10780 (Chen et al., 2010) and GSE21422 (Kretschmer et al., 2011) identified CDYL2 up-regulation in invasive ductal breast carcinomas as well as ductal carcinoma *in situ*, compared with normal breast tissues (Figure 1A). Analysis of the paired Clinical Proteomic Tumor Analysis Consortium (CPTAC) (Ellis et al., 2013) and TCGA datasets revealed that CDYL2 protein expression correlated with mRNA levels (Figure 1B). We found that both TCGA mRNA and CPTAC protein levels for CDYL2 across breast cancer subtypes also showed similar patterns, being higher in the ER+ forms than TN forms (Figures S1B and S1C). We next asked if the expression level of CDYL2 correlates with clinical outcome. Patients were subdivided into three categories based on their expression of the ER, PR, and HER2, namely, ER+/HER2−, ER+/HER2+, and receptor TN. This revealed that high expression of CDYL2 correlated with worse survival in both ER+/HER2− and TN subtypes (Figures 1C and 1D), but not ER+/HER2+ (Figure 1E). We also analyzed the expression of CDYL2 in normal breast tissues over the course of breast cancer progression, across all breast cancer types, ER+/HER2− and TN. This showed up-regulation of CDYL2 from the earliest pre-metastatic stage (pN0) in all three patient cohorts (Figures S1D–S1F). To further probe a possible association between CDYL2 expression and breast cancer progression, we examined its correlation with cancer gene expression signatures in the Molecular Signature Database (MSigDB) (Subramanian et al., 2005). This uncovered a positive correlation between CDYL2 expression in both ER+/HER2− and TN breast cancer and the Rizki_tumor_invasiveness-2D-UP signature (Figures S1G and S1H), corresponding to genes

A

Dataset	Patient Cohort	Fold Change	P-value	Tumor (n)	Normal (n)	Ref.
Oncomine TCGA Breast	Mixed Lobular and Ductal Breast Carcinoma	2.571	1.53E-10	7	61	Cancer Genome Atlas Network, 2012
Oncomine TCGA Breast	Invasive Lobular Breast Carcinoma	2.433	7.26E-16	36	61	Cancer Genome Atlas Network, 2012
Oncomine TCGA Breast	Invasive Ductal Breast Carcinoma	2.535	2.20E-31	289	61	Cancer Genome Atlas Network, 2012
Oncomine TCGA Breast	Invasive Breast Carcinoma	2.285	1.34E-16	76	61	Cancer Genome Atlas Network, 2012
GSE10780	Invasive Ductal Breast Carcinoma	1.395	1.13E-06	42	143	Chen *et al.*,2010
GSE21422	Ductal Carcinoma In Situ	3.41	1.99E-02	9	5	Kretschmer *et al.*, 2011
GSE21422	Invasive Ductal Carcinoma	5.521	1.63E-03	5	5	Kretschmer *et al.*, 2011

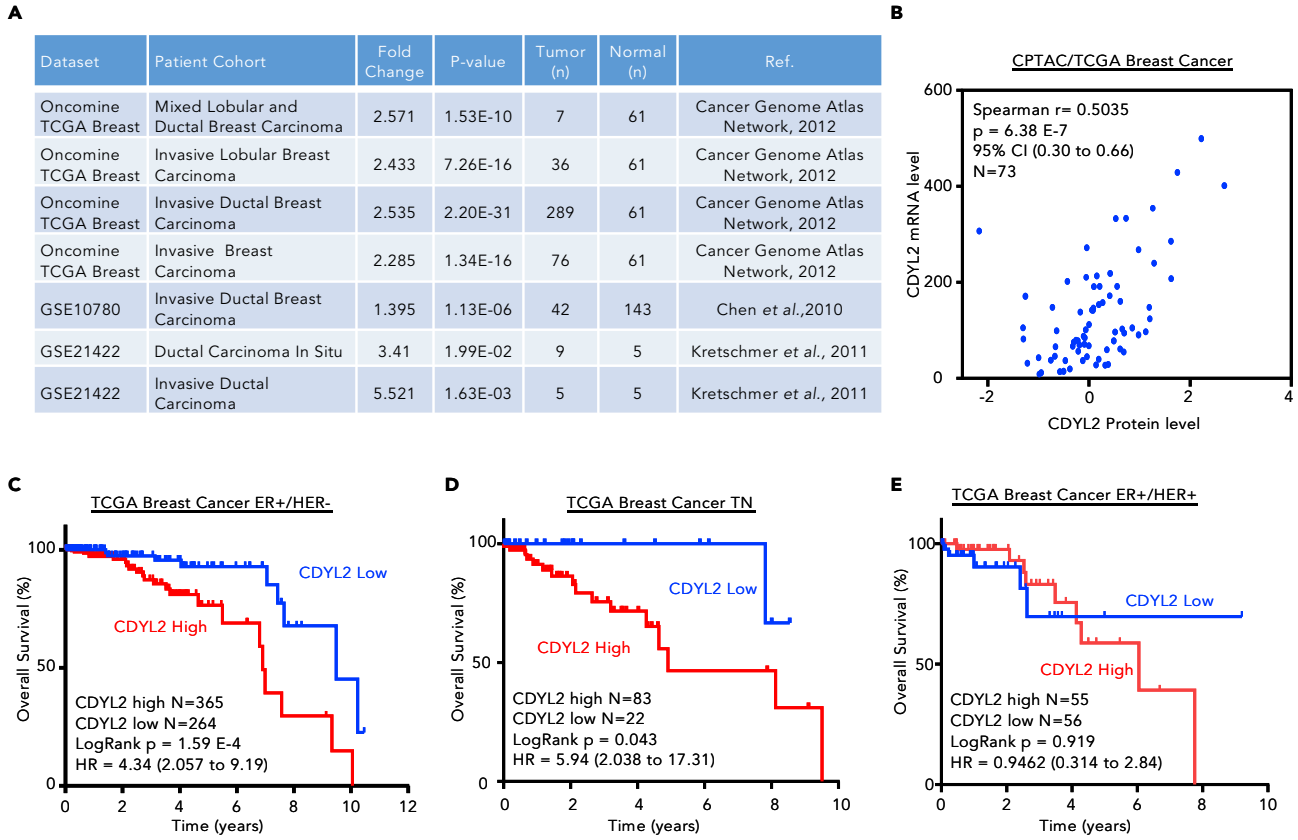

Figure 1. High CDYL2 Expression Level in Breast Cancer Is Associated with Poor Prognosis

(A) CDYL2 mRNA expression in breast tumors compared with normal tissues, as derived from the Oncomine database and GEO2R analysis of the indicated GEO datasets.

(B) Paired analysis of CDYL2 mRNA (TCGA, RNA-seq) and protein levels (CPTAC, mass spectrometry) in individual tumor specimen.

(C–E) Kaplan-Meier overall survival (OS) analysis performed from TCGA breast cancer subtypes: ER+/HER2− (C), triple negative (TN) (D), and ER+/HER2+ (E) using best cutoff of CDYL2 expression (high and low). Significance using log rank p value and hazard ratio (CI).

up-regulated in an invasive breast cancer cell line relative to the non-invasive precursor cell line from which it was derived (Rizki et al., 2008). Finally, we extended our analysis to other cancer contexts, revealing an association between CDYL2 expression level and survival in colorectal carcinoma, rectal adenocarcinoma, lung squamous cell carcinoma, and lung adenocarcinoma (Figures S1I–S1L). These findings identify *CDYL2* as a gene commonly up-regulated in breast cancer and a candidate modulator of cancer progression and patient survival in the ER+/HER2− and TN subtypes, and other cancer forms.

CDYL2 Over-Expression in the Non-invasive Breast Cancer Cell Line MCF7 Induces Transcriptional Changes Associated with Malignant Progression

To ask if CDYL2 up-regulation could induce oncogenic transcriptional and cellular changes, we stably expressed a CDYL2 cDNA in the non-invasive breast cancer cell line MCF7 (MCF7-CDYL2) or empty vector (MCF7-Vector) (Figure 2A). CDYL2 over-expression did not affect cell growth (Figure S2A), whereas RNA sequencing (RNA-seq) revealed striking differences between MCF7-CDYL2 and MCF7-Vector cells, with 693 genes up-regulated and 174 genes down-regulated at least 2.5-fold (Figure 2B; Table S1). Gene set enrichment analysis (GSEA) of genes up- or down-regulated in MCF7-CDYL2 cells revealed positive associations with EMT, metastasis, invasive versus non-invasive ductal carcinoma, breast cancer relapse in bone, and atypical ductal hyperplasia compared with non-cancerous breast tissue (Figures 2C and 2D). A number of genes from these GSEA signatures were validated by qRT-PCR, focusing on genes that are individually associated with breast cancer cell plasticity and malignant progression. These include the proto-oncogenes *SOX2, KLF4, MYC, MUC1, FOS, FOSL1/Fra-1,* and *JUN* (Alam et al., 2014; Bakiri et al., 2015; Jiao et al., 2010; Kufe, 2013; Nair et al., 2014; Piva et al., 2014; Yu et al., 2011), and the secretory

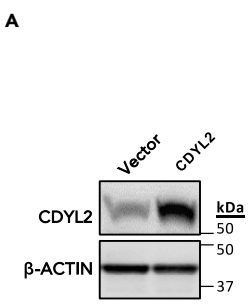

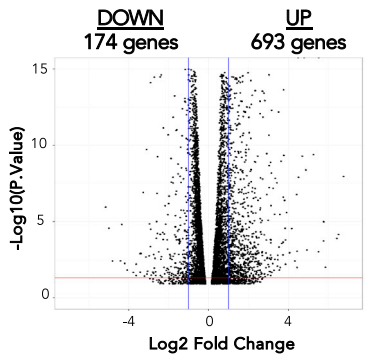

C

Over-Represented in UP-regulated Genes

Enriched Gene Set Name (# genes (K))	Description	Overla p (k)	k/K	p-value	FDR q-value
HALLMARK EPITHELIAL MESENCHYMAL TRANSITION (200)	Genes defining EMT, as in wound healing, fibrosis and metastasis.	25	0.125	1.96E-20	3.26E-19
CHARAFE BREAST CANCER LUMINAL VS MESENCHYMAL DN (460)	Down-regulated in luminal-like BC cells compared to the mesenchymal-like.	32	0.069	4.79E-18	4.22E-16
SCHUETZ BREAST CANCER DUCTAL INVASIVE UP (351)	Genes up-regulated in IDC relative to DCIS.	27	0.076	1.68E-16	9.63E-15
CHARAFE BREAST CANCER LUMINAL VS BASAL DN (455)	Down-regulated in luminal-like BC cells compared to the basal-like.	29	0.063	1.79E-15	8.18E-14

Over-Represented in Down-regulated Genes

Enriched Gene Set Name (# genes (K))	Description	Over-lap (k)	k/K	p-value	FDR q-value
JAEGER METASTASIS DN (258)	Genes down-regulated in metastases from malignant melanoma v's primary tumors.	13	0.05	4.38E-13	1.52E-10
SMID BREAST CANCER RELAPSE IN BONE DN (315)	Genes down-regulated in bone relapse of breast cancer.	10	0.031	2.05E-08	1.40E-06
POOLA INVASIVE BREAST CANCER DN (134)	Genes down-regulated in atypical ductal hyperplastic breast cancer tissues v's those without cancer.	6	0.044	2.13 E-08	7.93 E-07
CHANDRAN METASTASIS DN (306)	Genes down-regulated in metastatic prostate tumors.	8	0.026	2.38E-06	8.60 E-05

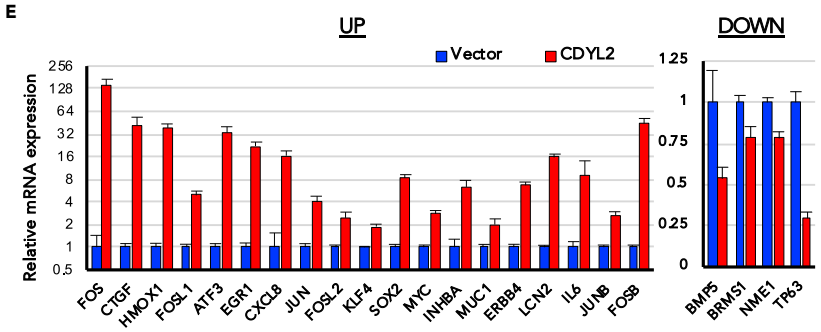

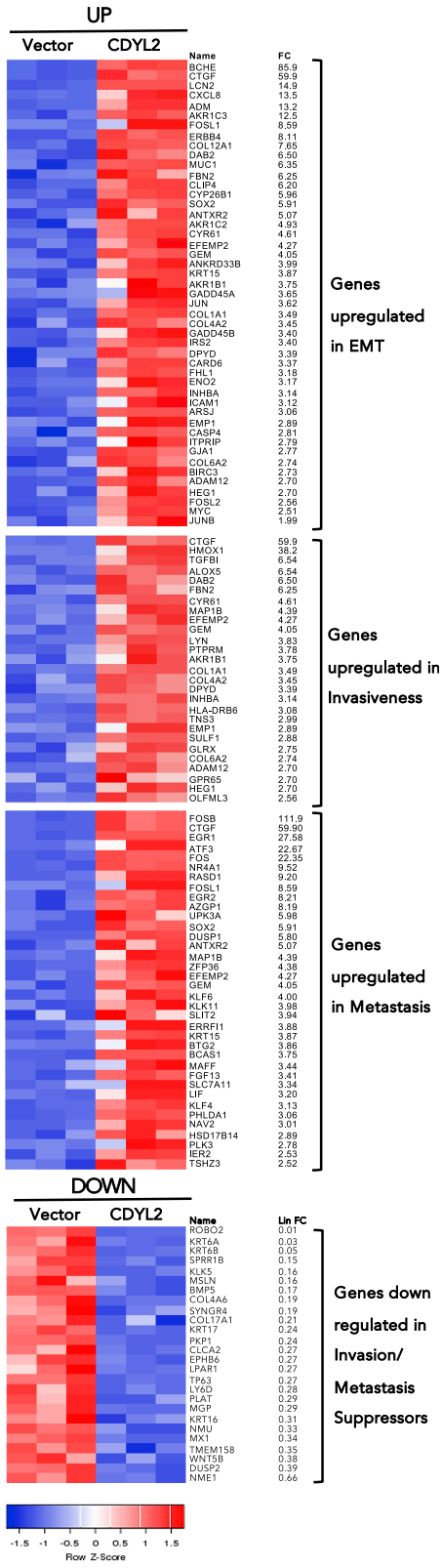

Figure 2. CDYL2 Over-Expression in the Non-invasive Breast Cancer Line MCF7 Induces Transcriptional Changes Associated with Malignant Progression

(A) Western blot analysis of CDYL2 and beta-actin expression in MCF7-CDYL2 and MCF7-Vector cells.

(B) Volcano plot showing genes up- or down-regulated at least 2.5-fold at an adjusted p value less than 0.05 (t test).

(C) Selected molecular signatures over-represented in either the up-or down-regulated gene sets from (B).

(D) Heatmap showing expression of genes from molecular signatures in (C) in the triplicate RNA-seqs.

(E) qRT-PCR validation of selected differentially expressed genes from (C). Mean of three independent experiments ±S.D. All differential expressions were significant at $p < 0.05$ (t test).

molecules *LCN2, CTGF, CXCL8, INHBA,* and *IL6* (Rhodes et al., 2004, p. 8; Shimo et al., 2006; Singh et al., 2013, 2013; Sullivan et al., 2009, p. 8) (Figure 2E). Down-regulation of the tumor suppressor *TP63,* breast cancer metastasis suppressor *BRMS1,* and cytokine *BMP5,* which regulate EMT, metastasis, and stemness, among other processes (Gatti et al., 2019; Romagnoli et al., 2012), was also confirmed (Figure 2E). Together, these insights suggest that CDYL2 over-expression can induce transcriptional changes associated with malignant breast cancer, potentially by promoting EMT, invasiveness, and metastasis.

CDYL2 Over-expression in MCF7 Cells Induces EMT-like Changes, Migration, Invasiveness, and Mammosphere Formation

Further probing if CDYL2 might induce EMT-like changes in MCF7 cells, we assessed the expression of a panel of established EMT markers. qRT-PCR analysis revealed CDYL2 up-regulation of mesenchymal markers TWIST1, SNAI1, FN1, VIM, CTNNB1, and SNAI2 (Figure 3A). Western blotting revealed down-regulation of epithelial marker E-Cadherin and up-regulation the mesenchymal markers Vimentin (VIM), TWIST1/Twist, and SNAI1/Snail (Figure 3B). However, CDYL2 over-expression did not alter the levels of ER-alpha (Figure 3B), down-regulation of which can induce EMT (Dhasarathy et al., 2007), suggesting an independent mechanism. Notably, 3 weeks after MCF7 cells were transduced with the CDYL2 over-expression construct a change in cell morphology occurred, with loss of the cobblestone-like morphology of monolayers, replaced by a more fibroblast-like morphology (Figure 3C), similar to previous descriptions of EMT in MCF7 (Lin et al., 2014; Yin et al., 2008).

To further investigate the possibility that CDYL2 over-expression induced EMT in MCF7 cells, we analyzed the expression of the cell surface adhesion molecules EpCAM and CD49f. It was previously demonstrated that low expression levels of EpCAM are associated with both EMT and breast cancer stem cells. The EpCAM−/CD49f− subpopulation of transformed mammary epithelial cells was especially tumorigenic, confirming high tumor-initiating, stem-like capacity. On the other hand, the EpCAM+/CD49f− subpopulation was shown not to form tumors (Kim et al., 2015). We found that over-expression of CDYL2 in MCF7 cells results in the appearance of a substantial population of EpCAM−/CD49f− cells (Figure S2C, top panels). Notably, CDYL2 over-expression also induced an EpCAM−/CD49f− cell population in another ER+ breast cancer cell line, Cama-1 (Figure S2C, center panels).

Among the primary contributions of EMT to malignant progression is increased cancer cell migration and invasion. *In vitro* assays revealed that the MCF7-CDYL2 cells migrated more proficiently across a microporous membrane compared with controls (Figures 3D and 3E). Using an adaptation of this assay to test for invasive capacity, wherein the porous membrane was first overlaid with a Matrigel barrier, we found that MCF7-CDYL2 cells also had increased invasive capacity relative to controls (Figure 3F).

We then probed the effect of CDYL2 on MCF7 cell invasion and metastasis *in vivo*. Both MCF7-CDYL2 and control cells were fluorescently labeled and injected into the perivitelline space of zebrafish embryos. The presence of tail metastases was monitored by fluorescence microscopy 24 h later. MCF7-Vector cells rarely produced metastases (3.57% of fish), whereas MCF7-CDYL2 cells did so in 21.57% of cases (Figure 3G).

To test if CDYL2 over-expression additionally induced stem-like characteristics in MCF7 cells, we first performed a mammosphere assay. This is a functional assay to assess the enrichment of stem-like cells in a population. MCF7-CDYL2 cells yielded both more and larger mammospheres compared with controls (Figures 3H–3J). Consistent with this, flow cytometry analysis revealed that CDYL2 over-expression in MCF7 cells increased the fraction of cells bearing the stem-like antigenic profile of CD44-high/CD24-low cells compared with controls (Figures 3K and 3L). Taken together, this series of studies indicates that CDYL2 over-expression in MCF7 cells promotes a number of cellular phenotypes associated with cellular plasticity and malignant progression.

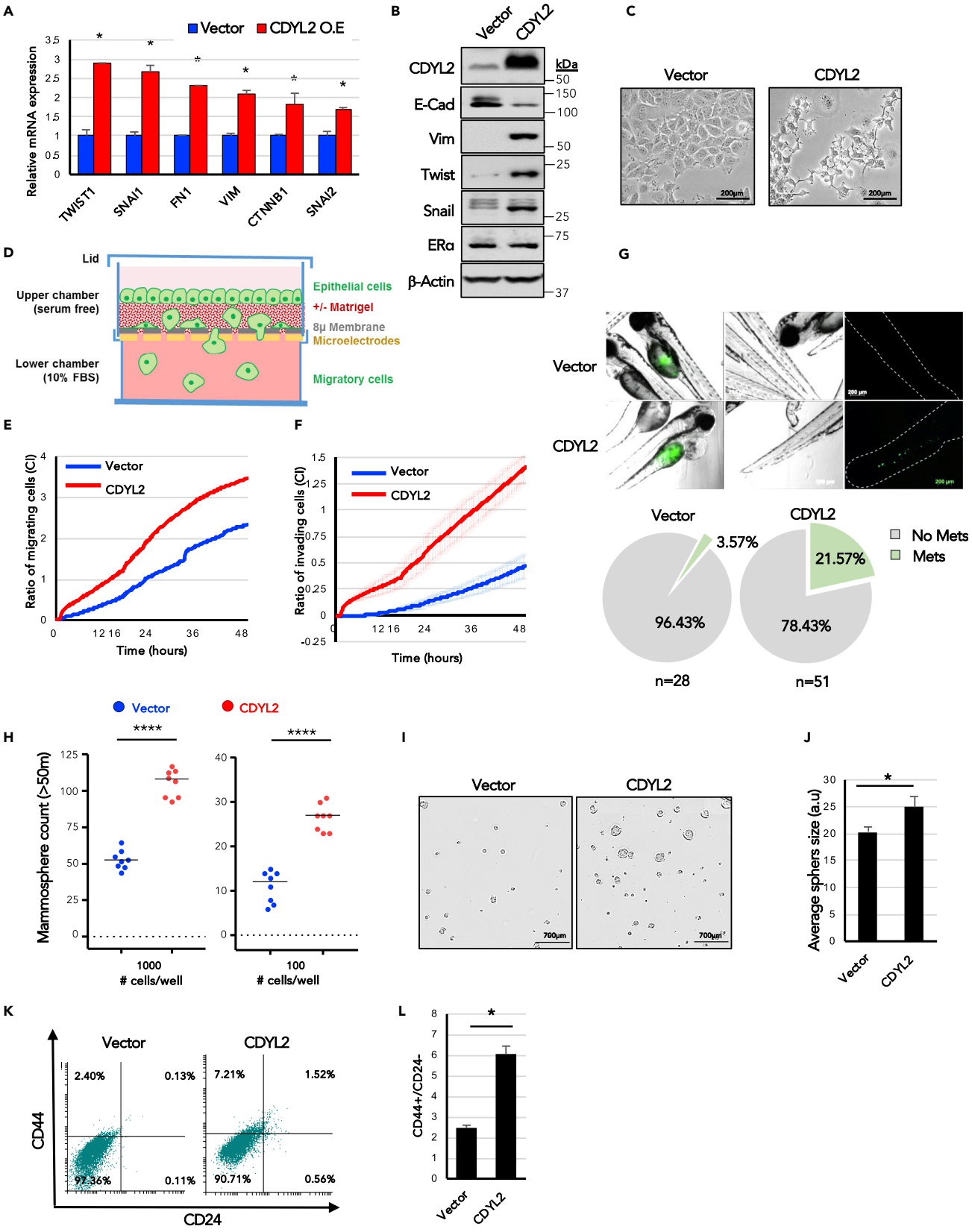
A
Vector
CDYL2 O.E
Relative mRNA expression
TWIST1
SNAI1
FN1
VIM
CTNNB1
SNAI2
B
Vector
CDYL2
kDa
CDYL2
E-Cad
Vim
Twist
Snail
ERα
β-Actin
C
Vector
CDYL2
200μm
D
Lid
Upper chamber
(serum free)
Lower chamber
(10% FBS)
Epithelial cells
+/- Matrigel
8μ Membrane
Microelectrodes
Migratory cells
E
Vector
CDYL2
Ratio of migrating cells (CI)
Time (hours)
F
Vector
CDYL2
Ratio of invading cells (CI)
Time (hours)
G
Vector
CDYL2
Vector
CDYL2
3.57%
96.43%
21.57%
78.43%
No Mets
Mets
n=28
n=51
H
Vector
CDYL2
****
****
Mammosphere count (>50m)
1000
cells/well
100
cells/well
I
Vector
CDYL2
700μm
J
Average spheres size (a.u)
Vector
CDYL2
K
Vector
CDYL2
2.40%
0.13%
97.36%
0.11%
7.21%
1.52%
90.71%
0.56%
CD44
CD24
L
CD44+/CD24-
Vector
CDYL2

Figure 3. CDYL2 Over-Expression in MCF7 Cells Induces EMT-like Changes, Accompanied by Increased Migration, Invasiveness, and Mammosphere Formation

(A) qRT-PCR analysis of a panel of EMT marker genes, normalization to GAPDH. Shown is mean ± SD of three experiments. Differences significant at $p < 0.05$ (t test).

(B) Western blot analysis of a panel of EMT markers, ER-alpha, CDYL2, and beta-actin.

(C) 10× phase contrast micrograph of MCF7-CDYL2 and MCF7-Vector control. Scale bar, 200 μM.

(D) Schematic diagram of the xCELLigence quantitative, real-time migration and invasion assay system.

(E) xCELLigence assay comparing the relative migration efficiency (Cell Index, CI) of MCF7-Vector and MCF7-CDYL2 cells. Both (E) and (F) show technical quadruplicates ± SD. Experiments were repeated at least three times with similar results.

(F) Invasion assays were performed as in (E), except that the porous membrane separating the upper and lower chambers of the transwell was first overlaid with Matrigel.

(G) Zebrafish embryo cell invasion and migration assay. Shown are micrographs illustrating the metastasis of fluorescently labeled MCF7-CDYL2 or MCF7-Vector from the site of injection to the tail. Scale bar, 200 μM. Quantification of the percentage of embryo exhibiting tail metastases is shown below. Experiments were repeated three times.

(H) Mammosphere formation in MCF7-CDYL2 cells compared with MCF7-Vector controls. Cells were plated at the indicated seeding number per well in 96-well plates. Mammospheres with size >50 μm were counted after 8 days. Shown is a scatterplot of the results of a representative of three independent experiments indicating the median (black bar) and t test significance (****$p < 0.0001$).

(I) Representative 4× phase microscopy images of mammospheres counted in (H). Scale bar, 700 μM.

(J) Mammosphere diameters were determined by image analysis. Shown is mean + SD of eight wells in which 1,000 cells were seeded. t test significance (*$p < 0.05$).

(K and L) FACS analysis of antigenic profile associated with breast cancer stem cells (CD44+; CD24-low/negative). Shown are representative FACS scatterplots (K) and the mean of three independent experiments ± S.D. (L). t test significance (*$p < 0.05$).

RNAi Knockdown of CDYL2 in the Invasive Breast Cancer Cell Line MDA-MB-231 Diminishes the Expression of EMT Markers and Inhibits Migration, Invasion, and Mammosphere Formation

We next analyzed the effect of CDYL2 loss of function in the highly invasive, cancer stem cell-enriched, mesenchymal-like breast cancer line MDA-MB-231. CDYL2 expression was inhibited by RNAi (Figures 4A and 4B) and high-throughput RNA-seq analysis performed. This revealed that compared with CDYL2 over-expression in MCF7 cells, the effects of its knock-down on MDA-MB-231 cell gene expression were more moderate, with no genes up- or down-regulated 2.5-fold or greater, except for CDYL2 itself (Table S2). However, using a fold-change cutoff of 1.25, we identified 204 genes up-regulated and 129 genes down-regulated (Figure 4C, Table S2). These gene lists were subjected to over-representation analysis using the GSEA molecular signatures database. This revealed that the down-regulated gene set was enriched in transcripts associated with EMT, metastasis, mammary stem cells, and invasive ductal carcinoma (Figures 4D and 4E). This suggests that CDYL2 knock-down might suppress EMT, metastasis, and stemness. To determine if this is the case, we performed essentially the same suite of assays used to probe the effect of CDYL2 over-expression on MCF7 cells (Figure 3).

We first confirmed by qRT-PCR that CDYL2 RNAi reduced the levels of a number of transcripts associated with EMT, namely, JUN, MYC, SNAI2, FOSL1, and TWIST1 (Figure 4F). Immunoblotting revealed induction of E-cadherin expression and diminished expression of Vimentin, Fibronectin, and Twist (Figure 4G). Fluorescence-activated cell sorting (FACS) analysis revealed that CDYL2 RNAi also induced the appearance of a subpopulation of EpCAM+/CD49− MDA-MB-231 cells (Figure S2C, lower panels), which was shown to be associated with loss of tumorigenicity (Kim et al., 2015). However, we did not observe morphological changes in these cells indicative of a mesenchymal-to-epithelial transition (MET), possibly because the duration of the RNAi treatment was not long enough for such phenotypes to emerge. Nonetheless, transduction of MDA-MB-231 cells with three independent small hairpin RNA (shRNA) sequences targeting CDYL2 (Figure S3A) did result in epithelial-like morphological changes after 2 weeks, with cells forming cobblestone-like monolayers (Figure S3B). These cells also exhibited down-regulation of a number genes associated with EMT induction that were strongly up-regulated in MCF7-CDYL2 cells (*FOS, FOSB, JUNB, CXCL8, CTGF, LCN2, MUC1, ERBB4*), but not down-regulated in MDA-MB-231 cells treated with transient CDYL2 RNAi (Figure S3C).

The effect of CDYL2 RNAi on motility and invasiveness of MDA-MB-231 cells was evaluated using *in vitro* assays, revealing that transient or stable RNAi of CDYL2 dramatically reduced the migratory and invasive ability of MDA-MB-231 cells, relative to controls (Figures 4H, 4I, S3D, and S3E). *In vivo*, CDYL2 RNAi significantly impaired the ability of MDA-MB-231 cells to metastasize from the perivitelline site of injection to the tail of zebrafish embryos (Figure 4J), indicating suppression of the invasive and/or migratory capacity. Knockdown of CDYL2 by transient or stable RNAi treatment also resulted in fewer and smaller mammospheres relative to negative controls (Figures 4K–4M and S3F). While FACS analysis revealed that the

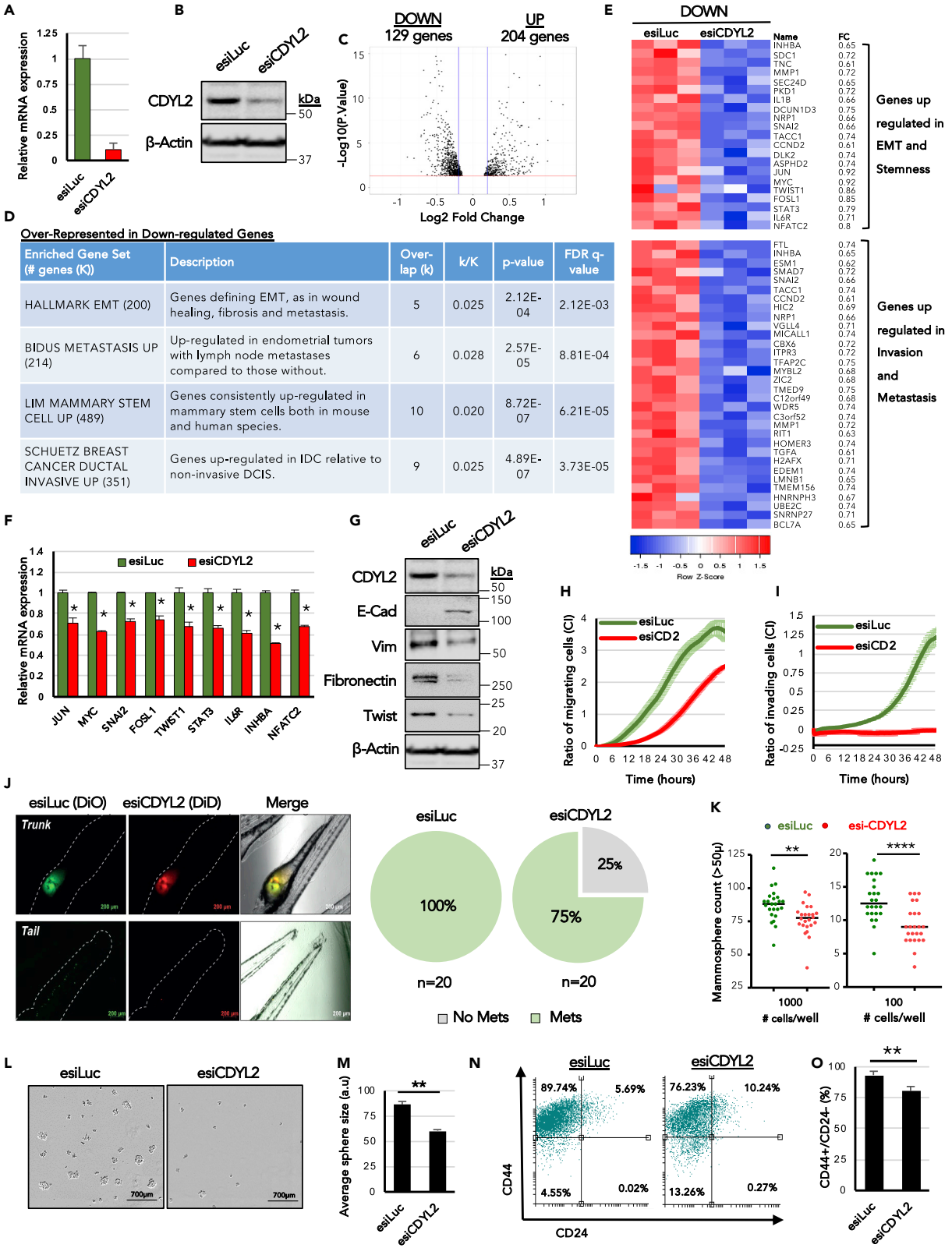

Enriched Gene Set (# genes (K))	Description	Over-lap (k)	k/K	p-value	FDR q-value
HALLMARK EMT (200)	Genes defining EMT, as in wound healing, fibrosis and metastasis.	5	0.025	2.12E-04	2.12E-03
BIDUS METASTASIS UP (214)	Up-regulated in endometrial tumors with lymph node metastases compared to those without.	6	0.028	2.57E-05	8.81E-04
LIM MAMMARY STEM CELL UP (489)	Genes consistently up-regulated in mammary stem cells both in mouse and human species.	10	0.020	8.72E-07	6.21E-05
SCHUETZ BREAST CANCER DUCTAL INVASIVE UP (351)	Genes up-regulated in IDC relative to non-invasive DCIS.	9	0.025	4.89E-07	3.73E-05

Figure 4. RNAi Knockdown of CDYL2 in the Invasive Breast Cancer Cell Line MDA-MB-231 Induces Transcriptional and Phenotypic Changes Associated with Inhibition of Malignancy

(A and B) CDYL2 knock-down validated by RT-qPCR (A) and western blotting (B).

(C and D) (C) Volcano plot showing genes up- or down-regulated at least 1.25-fold. (D) Selected molecular signatures from the MSigDB database that were over-represented in either the up- or down-regulated gene sets from (C).

(E) Heatmap showing expression of selected genes from (D) in the triplicate RNA-seq.

(F) qRT-PCR validation of differential expression of selected genes from (D). Expression normalized to GAPDH. Data are the mean ± SD of three independent experiments. All differential expressions significant at $p < 0.05$ (t test).

(G) Western blot analysis of a panel of EMT markers, CDYL2, and beta-actin.

(H) xCELLigence assay comparing the relative migration efficiency of MDA-MB-231 cells treated with esiLuc or esiCDYL2 (esiCD2). Both (H) and (I) show technical quadruplicates ± SD. Experiments were repeated at least three times with similar results.

(I) Invasion assays were performed as in (H), except that the porous membrane separating the upper and lower chambers of the transwell was first overlaid with Matrigel.

(J) Fluorescence microscopy analysis of with esiLuc or esiCDYL2 on the migration of MDA-MB-231 from the perivitelline space of zebrafish embryos to the tail. Representative images are shown. Scale bar, 700 μM. Quantification of the percentage of embryos exhibiting tail metastases (Mets) is shown to the right. Experiments were repeated three times with similar results.

(K) Mammosphere formation in MDA-MB-231 cells treated with esiLuc or esiCDYL2. Cells were plated at the indicated seeding number per well in 96-well plates. Mammospheres with size >50 μm were counted after 8 days. Shown is a scatterplot of the results of a representative of three independent experiments indicating the median (black bar) and t test significance (**$p < 0.01$; ****$p < 0.0001$).

(L) Representative 4× phase microscopy images of mammospheres counted in (K) are shown. Scale bar, 200 μM.

(M) The diameters of mammospheres from (K) were determined using image analysis software. Shown is the mean +SD of eight wells in which 1,000 cells were seeded. t test significance (**$p < 0.01$).

(N and O) FACS analysis of antigenic profile associated with breast cancer stem cells (CD44+; CD24-low/negative). Shown are representative FACS scatterplots (N) and the mean of three independent experiments ± SD. (O). t test significance (**$p < 0.01$).

majority of control RNAi-treated MDA-MB-231 cells were CD44-high/CD24-low, CDYL2 RNAi induced a population of CD44-low/CD24-low cells, indicative of loss of stemness (Figures 4N, 4O, and S3G). Collectively, these assays indicate that CDYL2 is required for MDA-MB-231 cell migration, invasion, and stemness, as well as the full expression of its mesenchymal-like state.

Regulation of p65/NF-κB and STAT3 Signaling by CDYL2

Gene expression signature analysis of the effects of CDYL2 over-expression in MCF7 cells or knockdown in MDA-MB-231 revealed a potential role in regulating NF-κB/TNF-alpha and STAT3/interleukin-6 signaling (Figure 5A). Given the importance of these signaling pathways in controlling cancer cell EMT, stemness, motility, and invasiveness, we asked if their regulation by CDYL2 might contribute to its regulation of these cellular processes. Consistent with the transcriptomic analysis, over-expression of CDYL2 in MCF7 cells increased the levels of tyrosine 705-phosphorylated STAT3 (Figure 5B), the active form of this protein. It also increased the levels of serine 536 phosphorylation on the NF-κB TF p65 (Figure 5B), indicating an increase in canonical NF-κB pathway signaling. By contrast, the levels of both phosphoproteins were diminished in CDYL2 RNAi-treated MDA-MB-231 cells (Figure 5C). We also probed the levels of total p65 and STAT3 proteins, as well as beta-actin, as a loading control. The total p65 levels were not affected by either CDYL2 over-expression or RNAi, whereas total STAT3 levels were higher in MCF7-CDYL2 cells compared with controls (Figure 5B) and down-regulated after CDYL2 RNAi in MDA-MB-231 cells (Figure 5C).

We then asked if CDYL2 induction of genes associated with EMT, invasion, and stemness in MCF7 cells might be dependent on signaling via p65/NF-κB and STAT3. STAT3 and p65 were knocked down by transient transfection with small interfering RNA (siRNA) in both MCF7-Vector and MCF7-CDYL2 cells. A non-targeting siRNA was used as a control (Figures 5D and 5E). qRT-PCR analysis then revealed that p65 RNAi down-regulated several genes associated with NF-κB signaling, namely, *CTGF, EGR1, FOS, IL6, CXCL8, INHBA, JUN, MYC, SNAI1, KLF4, SOX2,* and *TWIST1* (Figure 5F). Similarly, STAT3 RNAi down-regulated several genes associated with STAT3 signaling, including *FOS, TWIST1, SOX2, JUN, MUC1, INHBA, IL6R, IL6ST,* and *TNF* (Figure 5G). Strikingly, RNAi knockdown of either p65 or STAT3 potently suppressed both invasiveness (Figures 5H and 5I) and mammosphere induction by CDYL2 (Figures 5J and 5K). Taken together, these analyses indicate that p65/NF-κB and STAT3 signaling is regulated by CDYL2, and that both pathways are required for CDYL2 induction of invasion and mammosphere formation in MCF7 cells.

CDYL2 Binds Upstream of *MIR124* Genes and Regulates miR-124 Expression

Consistent with the possibility that CDYL2 might be an epigenetic regulator of transcription, we found that it was enriched in the nucleus of both MCF7 and MDA-MB-231 cells, with a significant fraction present in the

A

Cell- Line	Input Gene List	Enriched Gene Set Name (# genes (K))	Description	# Genes in Over-lap (k)	k/K	p-value	FDR q-value
MCF7	Up-regulated in MCF7-CDYL2	HALLMARK TNFA SIGNALING VIA NFKB (200)	Genes regulated by NF-kB in response to TNF.	40	0.2	1.97E-40	9.86E-39
MCF7	Up-regulated in MCF7-CDYL2	STAT3 02 (147)	Genes having at least one occurrence of the transcription factor binding site V$STAT3 02 (v7.4 TRANSFAC) in the regions spanning up to 4 kb around their transcription starting sites.	14	0.095	2.03E-10	3.2E-09
MDA-MB-231	Down-regulated by esiCDYL2	HALLMARK TNFA SIGNALING VIA NFKB (200)	Genes regulated by NF-kB in response to TNF.	7	0.035	1.23E-06	2.06E-05
MDA-MB-231	Down-regulated by esiCDYL2	DASU IL6 SIGNALING UP (59)	Genes up-regulated in normal fibroblasts in response to IL6.	4	0.067	1.98E-05	7.25E-04

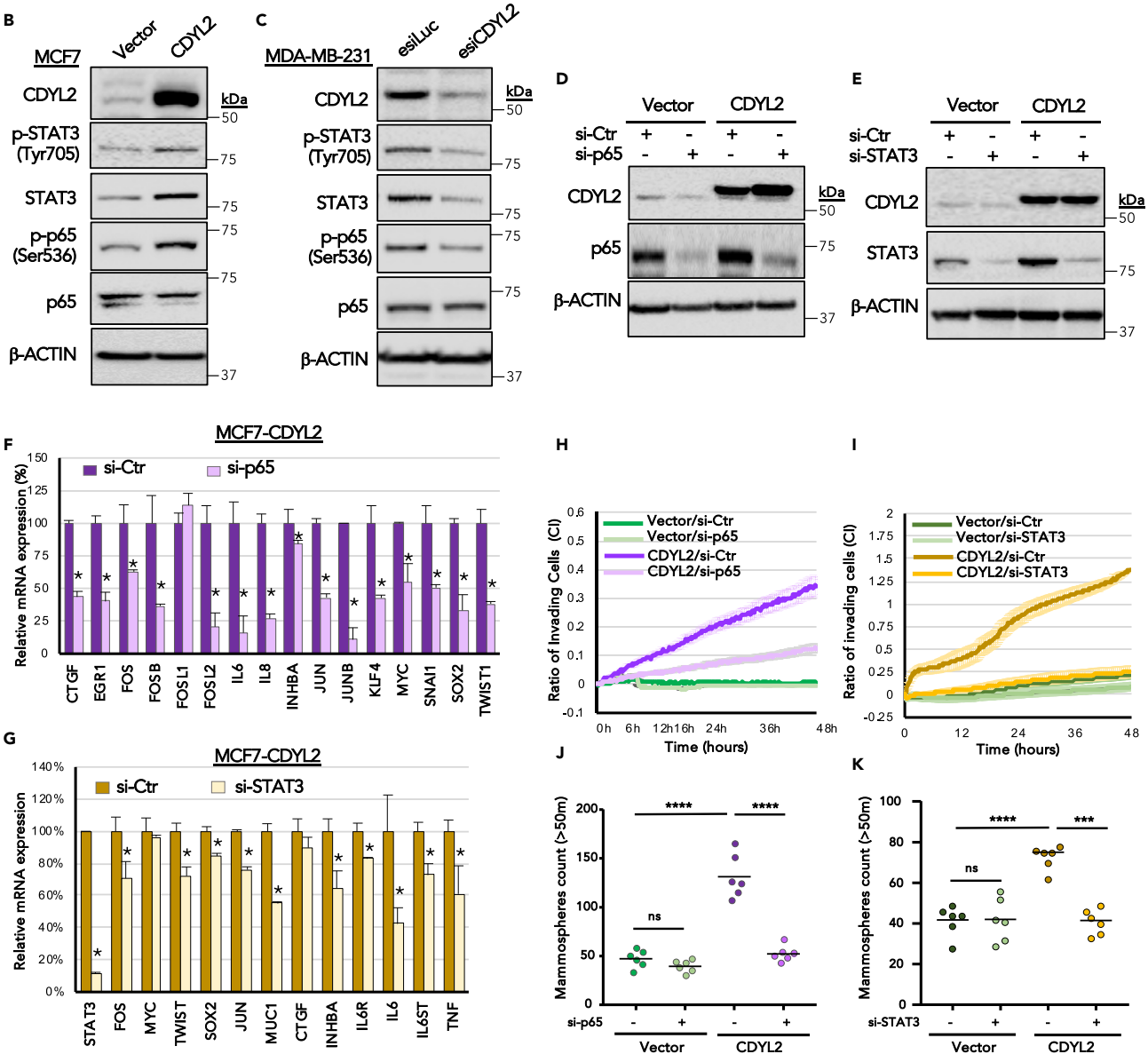

Figure 5. CDYL2 Regulation of NF-κB and STAT3 Signaling Contributes to Its Induction of Invasion and Mammosphere Formation

(A) Selected gene expression signatures enriched in the indicated RNA-seq datasets.

(B) Western blot of Ser536-phosphorylated p65 and Tyr705-phosphorylated STAT3 in MCF7-Vector versus MCF7-CDYL2. The levels of total p65, STAT3, and β-actin were also probed.

(C) As for (B), except comparing MDA-MB-231 cells treated with esiLuc or esiCDYL2.

(D and E) Western blot validation of RNAi knockdown of p65 (D) or STAT3 (E) in MCF7-Vector and MCF7-CDYL2 cells. β-actin is shown as loading control.

(F) qRT-PCR analysis of the effect of RNAi knockdown of p65 on the expression of a panel of NF-κB target genes that were up-regulated in MCF7-CDYL2 compared with MCF7-Vector cells. Data are represented as mean of three independent experiments ± SD. All differences were significant at $p < 0.05$ (t test).

(G) As in (F), except the effect of RNAi knockdown of STAT3 on the expression of a panel of its target genes up-regulated in MCF7-CDYL2 compared with MCF7-Vector cells was evaluated.

(H and I) xCELLigence invasion assays of MCF7-CDYL2 in MCF7 cells treated with either control RNAi or siRNA targeting p65 (H) or STAT3 (I). Graphs are representative of three independent experiments in quadruple runs per condition. Error bars represent the SD of quadruplicate readings at each time point.

(J and K) Mammosphere assay of MCF7-CDYL2 in MCF7 cells treated with either control RNAi or siRNA targeting p65 (J) or STAT3 (K). Mammospheres from 1,000 seeded cells with size >50 μm were counted after 8 days. Shown is a scatterplot of the results of a representative of three independent experiments indicating the median (black bar) and t test significance (***$p < 0.001$; ****$p < 0,0001$; ns, not significant).

chromatin fraction (Figures S4A–S4C). To identify where on chromatin CDYL2 is bound, we performed CDYL2 chromatin immunoprecipitation (ChIP) in both MCF7-Vector and MCF7-CDYL2 cells followed by Illumina sequencing (ChIP-seq). This revealed several genomic loci that were more enriched in CDYL2 in the MCF7-CDYL2 cells compared with vector controls, including upstream of all three members of the *MIR124* gene family (Figure 6A; Data S1, S2, and S3). Owing to their implication in tumor suppression, and the ability to regulate both p65/NF-κB and STAT3 signaling, EMT, invasion, and stemness (Cao et al., 2018; Hatziapostolou et al., 2011; Ji et al., 2019; Lv et al., 2011; Mehta et al., 2017; Olarerin-George et al., 2013; Wang et al., 2016a, 2016b), we decided to investigate CDYL2 regulation of the MIR124 genes further. We confirmed CDYL2 enrichment upstream of *MIR124* genes using ChIP-qPCR (Figure 6B). A non-reactive IgG was used as negative ChIP control, whereas qPCR analysis did not detect enrichment of CDYL2 at an unrelated sequence (Figure 6B). We reasoned that CDYL2 repression of *MIR124* genes might contribute to its regulation of STAT3 and NF-κB signaling in MCF7 and MDA-MB-231 cells. In agreement with this possibility, CDYL2 RNAi diminished its levels upstream of *MIR124* genes in MDA-MB-231 (Figure 6C), with a corresponding increase in the expression of both the precursor (pri-mir-124) and mature (miR-124-3p) forms of microRNA-124 (Figure 6E). Stable knock-down of CDYL2 using three independent shRNAs also increased levels of both pre-mir-124 and miR-124-3p (Figure S5). In complementary analysis, both *MIR124* transcripts were down-regulated by CDYL2 over-expression in MCF7 (Figure 6D). Supporting the notion that the alterations of miR-124 levels were sufficient to affect cell function, analysis of the MCF7-CDYL2 and MDA-MB-231 esiCDYL2 RNA-seq data showed that miR-124 target genes were commonly up-regulated in the former and down-regulated in the latter (Figure 6F). The miR-124 GSEA signature was also positively correlated with CDYL2 mRNA expression across all samples in the TCGA breast cohort, as well as in the ER+/HER2− and TN subtypes (Figures 6G–6I). Differential expression of several of the genes up-regulated in MCF7-CDYL2 cells or down-regulated in MDA-MB-231 cells treated with CDYL2 RNAi was validated by RT-qPCR (Figures 6J and 6K). In suppression assays, a miR-124-3p mimic strongly diminished the levels of the active, phosphorylated forms of both p65 and STAT3 (Figure 6L). miR-124-3p also suppressed the total levels of STAT3 protein (Figure 6L). In complementary experiments, a neutralizing anti-miR-124-3p oligonucleotide rescued esiCDYL2 suppression of phospho-p65 and phospho-STAT3 levels in MDA-MB-231 cells, compared with a control non-targeting anti-miR oligonucleotide (Figure 6M). The reduced total STAT3 levels observed upon esiCDYL2 treatment were also rescued by anti-miR-124-3p treatment (Figure 6M). These findings indicate that CDYL2 regulates miR-124 levels, possibly by its binding upstream of *MIR124* genes, and that control of miR-124-3p levels by CDYL2 contributes to its regulation of NF-κB and STAT3 signaling.

CDYL2 Interacts with G9a, GLP, and PRC2 Complex Components EZH2 and SUZ12

Because CDYL2 is enriched at *MIR124* genes and negatively regulates miR-124 expression, we asked if it might promote an epigenetically repressive chromatin environment at these loci. However, the epigenetic mechanism of CDYL2 is not known. By analogy with CDYL1, we speculated that it may form a complex with the H3K9 di-methyltransferases G9a, GLP, or SETDB1 (Mulligan et al., 2008) and the Polycomb Repressive Complex 2 (PRC2) core components EZH2 and SUZ12 (Zhang et al., 2011). Using immunoprecipitation (IP) assays we found that anti-CDYL2, but not a control IgG, efficiently recovered endogenous CDYL2 from MCF7 lysates and co-immunoprecipitated (coIP) G9a and its heterodimeric partner (Tachibana et al., 2005), GLP (Figure 7A). After long exposure of the western blot membrane, we also detected the presence of small amounts of EZH2 and SUZ12 in the CDYL2 IP, but at a much lower percentage of input compared

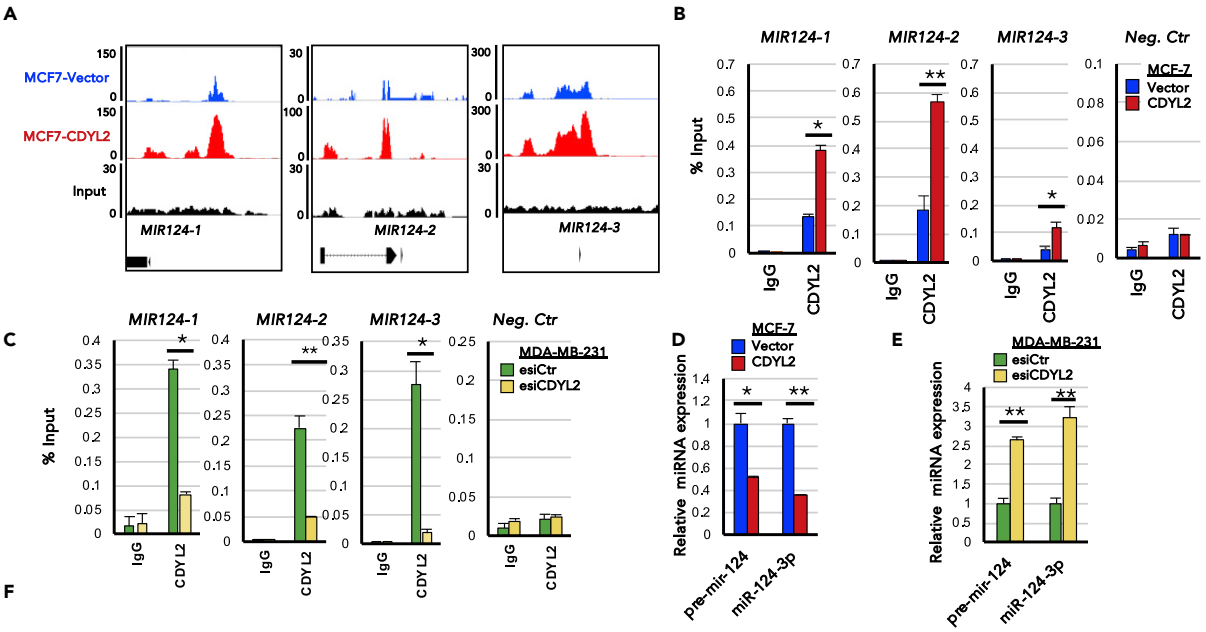

F

Gene set	Gene Set Name (# genes (K))	Over-lap (k)	k/K	p-val.	FDR
Up-regulated in MCF7-CDYL2	TGCCTTA MIR124A [a] (552)	18	3.20E-02	8.96E-06	8.25E-05
Down-regulated in MDA-MB-231 CDYL2 RNAi	TGCCTTA MIR124A [a] (552)	10	1.80E-02	2.57E-06	6.31E-05

[a] Genes having at least one occurrence of the motif TGCCTTA in their 3' untranslated region. The motif represents putative target (that is, seed match) of human mature miRNA hsa-miR-124a (v7.1 miRBase).

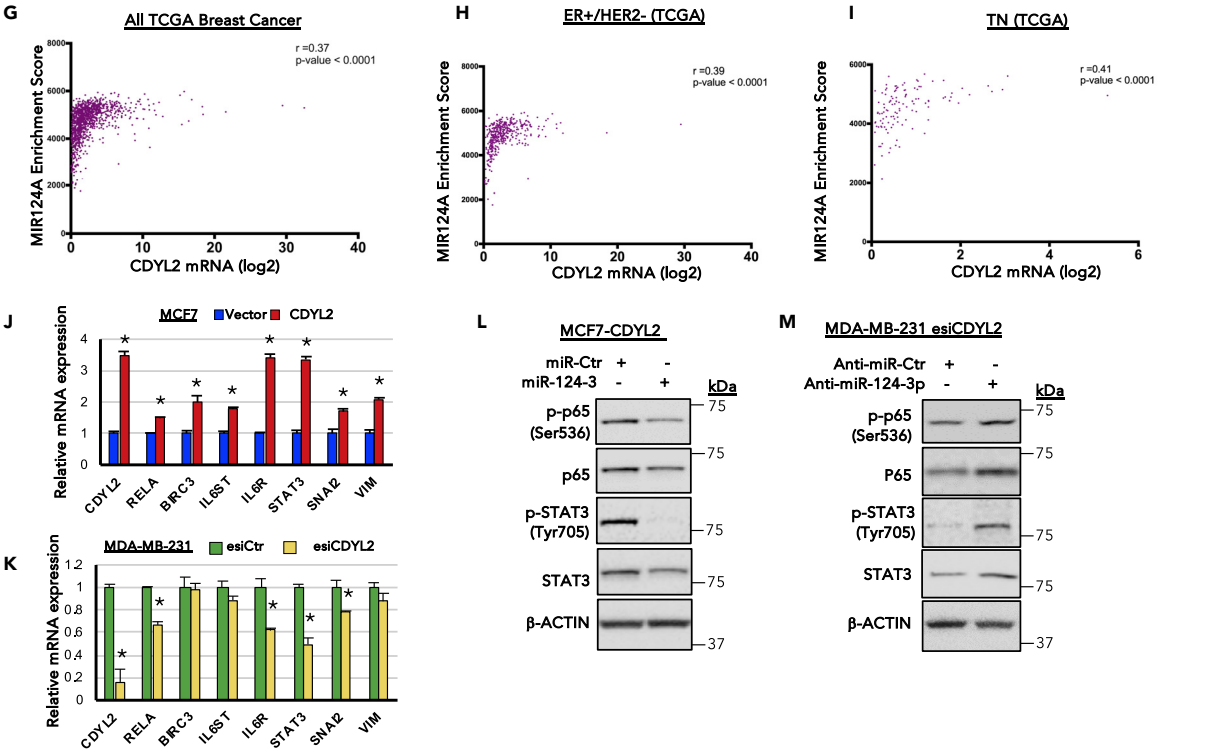

Figure 6. CDYL2 ChIP-Seq Analysis Identifies miR-124 as a Mediator of CDYL2 Regulation of STAT3 and NF-κB Signaling

(A) Relative enrichment of CDYL2 upstream of *MIR124* genes in MCF7-Vector cells (blue) and MCF7-CDYL2 (red), as revealed by ChIP-seq analysis. Input control and gene positions relative to the peaks are shown below.

(B) ChIP-qPCR validation of data presented in (A). ChIP-qPCR signal at an unrelated negative control sequence is also shown. Shown is the mean enrichment as a percentage of input of three independent experiments, ± SD. (*$p < 0.05$; **$p < 0.01$, t test)

(C) As in (B), except CDYL2 or IgG ChIP was performed using chromatin prepared from MDA-MB-231 cells treated with esiLuc or esiCDYL2.

(D) qRT-PCR analysis of pre-mir-124 and miR-124-3p levels in MCF7-CDYL2 and MCF7-Vector cells. Expression was normalized to an unrelated miRNA. Data represent the mean of three independent experiments ± SD. Significance determined by test (*$p < 0.05$; **$p < 0.01$).

(E) As in (D), except qRT-PCR analysis was performed using microRNA (miRNA) prepared from MDA- MB-231 cells treated with esiLuc or esiCDYL2.

(F) Selected gene expression signatures enriched in the indicated RNA-seq datasets.

(G–I) Correlation between CDYL2 expression and the GSEA signature "TGCCTTA MIR124A" in the indicated TCGA breast cancer patient cohorts. The linear regression r and p value are indicated.

(J) qRT-PCR analysis of the expression of miR-124-3p target genes in MCF7-CDYL2 and MCF7-Vector cells. Data represented as mean of three independent experiments ± SD. (*$p < 0.05$, by t test).

(K) As in (J), except qRT-PCR analysis was performed using RNA prepared from MDA-MB-231 cells treated with esiLuc or esiCDYL2.

(L and M) Western blot of phosphorylated p65 (Ser 536), total p65, phosphorylated STAT3 (Tyr 705), and total STAT3 in MCF7-CDYL2 cells treated with a miR124-3p mimic or miR control (L) or in MDA-MB-231 cells co-treated with esiCDYL2 and either an anti-miR-124-3p oligonucleotide or a control anti-miR (M). Data are representative of three independent experiments.

with G9a and GLP, suggesting a low abundance or labile interaction (Figure S6A). Reciprocal coIP assays confirmed G9a interaction with CDYL2, but did not identify CDYL2 association with EZH2 (Figures 7A and S6A). These data indicate that CDYL2 forms a complex with G9a and GLP and may interact marginally with EZH2 and SUZ12.

CDYL2 Regulates the Enrichment of G9a and EZH2 Upstream of *MIR124* Genes, as well as that of Their Cognate Methylation Marks H3K9me2 and H3K27me3

We next asked if CDYL2 might control the levels of G9a and EZH2 at a promoter-proximal region upstream of *MIR124* genes. ChIP-qPCR assays indicated that CDYL2, G9a, and EZH2 were enriched upstream of all three *MIR124* genes in both MCF7 and MDA-MB-231 cells (Figures 7B, 7C, S6B, and S6C). The enrichment of both methyltransferases was increased by CDYL2 over-expression in MCF7 cells (Figures 7B and S6B) and diminished by CDYL2 RNAi knockdown in MDA-MB-231 cells (Figures 7D and S6C). Increased levels of H3K9me2 and H3K27me3 were also observed upstream of *MIR124* genes in MCF7-CDYL2 (Figures 7C and S6B), whereas levels of H3K9me2 and H3K27me3 at these loci were decreased upon CDYL2 RNAi in MDA-MB-231 (Figures 7E and S6C). The levels of total histone H3 at these loci were not affected by CDYL2 over-expression in MCF7 or its knockdown in MDA-MB-231 (Figures 7C and 7E, left panels). The same pattern of alterations was not observed at two independent control sequences (Figures 7C and 7E, right panels; Figures S6B and S6C). These findings indicate that in addition to interacting with G9a, and weakly so with EZH2, CDYL2 positively regulates the enrichment of both methyltransferases upstream of *MIR124* genes, as well as those of the histone marks they regulate. To further probe the involvement of G9a and EZH2 in CDYL2 down-regulation of miR-124 levels, we treated MCF7-CDYL2 cells with the G9a/GLP inhibitor UNC0642 (Kim et al., 2017) or the EZH2 inhibitor CPI-169 (Bradley et al., 2014). We observed that UNC0642 treatment indeed resulted in increased levels of miR-124-3p (Figure S7A), relative to vehicle controls. However, treatment with CPI-169 at a range of doses did not affect miR-124-3p levels after 3, 4, or 5 days of treatment (Figure S7B and data not shown). This result further supports the importance of G9a/GLP methyltransferase activity in regulating miR-124 levels, but argues that inhibition of EZH2 enzymatic activity is not sufficient to antagonize CDYL2-mediated miR-124 down-regulation.

DISCUSSION

Despite the emergence of epigenetic factors as important regulators of cancer cell plasticity and malignant progression, the underlying molecular mechanisms remain poorly understood. This is due in part to insufficient characterization of several putative epigenetic factors, including CDYL2. Our study shows that CDYL2 is frequently misexpressed in breast cancer and provides a proof of principle that this could promote cellular phenotypes associated with malignant progression. We present the first insights into the genes and cellular pathways of CDYL2 controls, and the epigenetic mechanisms it engages. Based on our findings, we propose that CDYL2 up-regulation contributes to poor prognosis in breast cancer by inducing epigenetic deregulation of genes and pathways important in tumorigenesis (*MIR124*, NF-κB, STAT3), resulting in cellular changes central to malignant progression (EMT, migration, invasion, stemness) (schematic diagram, Figure 7F).

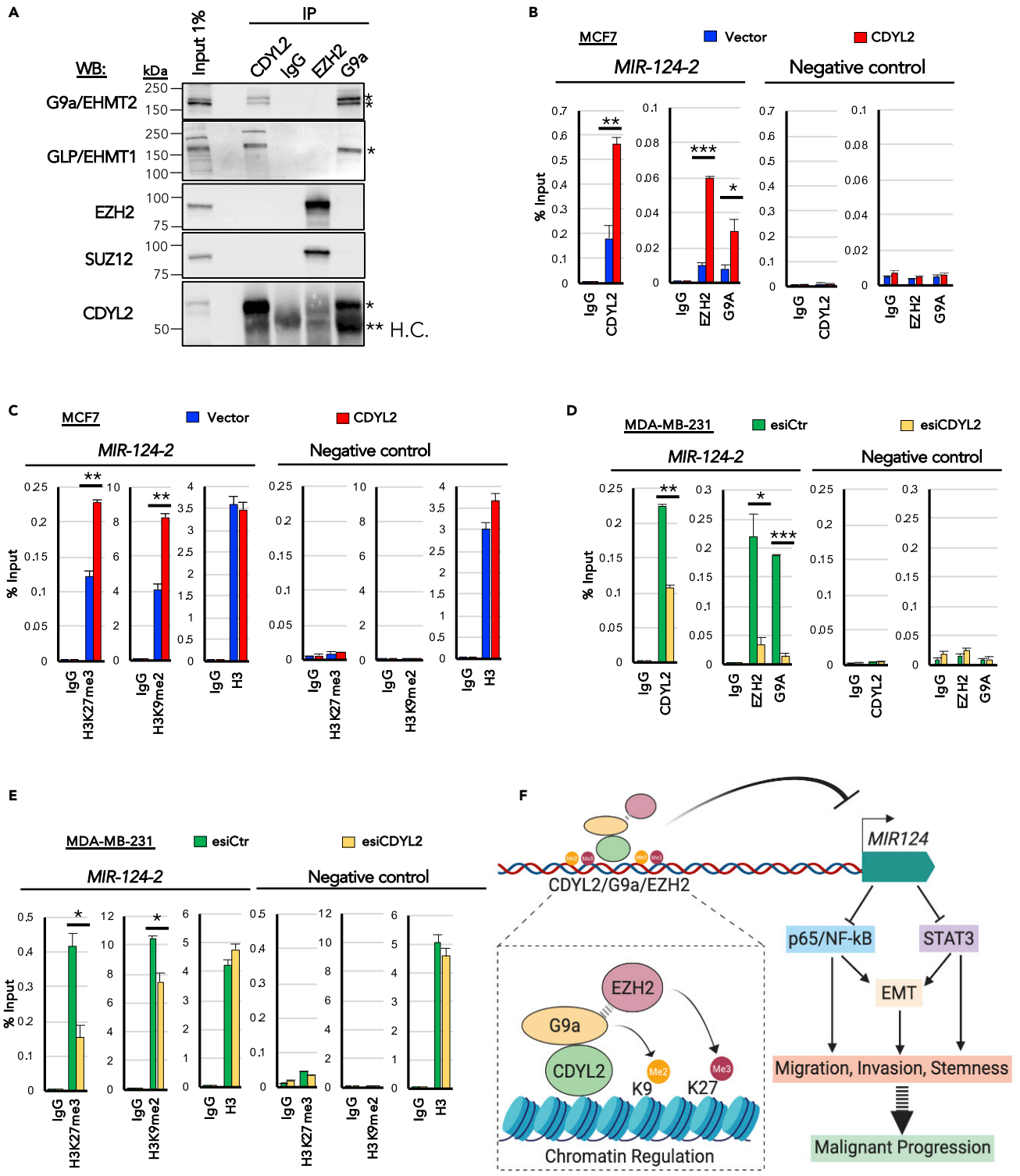

Figure 7. CDYL2 Interaction with G9a, GLP, EZH2, and SUZ12 and Its Regulation of G9a, EZH2, H3K9me2, and H3K27me3 Levels Upstream of *MIR124-2*

(A) Immunoprecipitation (IP) of CDYL2, EZH2, and G9a was performed on MCF7 cell lysates and the presence of the indicated proteins in the resulting IP eluates determined by western blotting (WB). A non-specific IgG was used as negative control. Input lysate was used to assess the relative strength of each coIP signal. The experiment was repeated three times with similar results. (*specific band; **H.C., IgG heavy chain).

Figure 7. *Continued*

(B) ChIP-qPCR analysis of the relative occupancy of CDYL2, EZH2, and G9a upstream of *MIR124-2* in MCF7-CDYL2 compared with MCF7-Vector cells. IgG, negative control ChIP. qPCR analysis was also performed at an unrelated negative control sequence. Shown is the mean enrichment as a percentage of input of three independent experiments, ± SD. Significance was determined by t test (*$p < 0.05$; **$p < 0.01$; ***$p < 0.001$).

(C) As in (B), except using antibodies specific to H3K9me2, H3K27me3, H3, and IgG. These ChIP analyses were conducted using the same lysates as in (B), so are paired analyses.

(D and E) Experiments were conducted as described in (B) and (C), except using chromatin lysates prepared from MDA-MB-231 cells treated with esiCDYL2 or esiLuc.

(F) Schematic model of the proposed contribution of CDYL2 to epigenetic regulation of MIR124, cell signaling, and malignancy-associated cellular processes.

Although we predicted CDYL2 to be an epigenetic repressor of transcription due to its homology to CDYL1 (Dorus et al., 2003; Fischle et al., 2008), this was not previously demonstrated. We have shown that CDYL2 is localized in the nuclear fraction of cells and binds to chromatin upstream of the *MIR124* genes. Further implicating CDYL2 as an epigenetic repressor of transcription, CDYL2 over-expression in MCF-7 cells both increased its enrichment upstream of *MIR124* genes and decreased the levels of *MIR124* transcripts. Treatment of MCF7-CDYL2 cells with the G9a/GLP inhibitor UNC0642 increased expression of miR-124-3p, indicating that the catalytic activity of G9a and/or its heterodimeric partner GLP (Tachibana et al., 2005) is important for the CDYL2-mediated repression of *MIR124* genes. Meanwhile, CDYL2 RNAi in MDA-MB-231 cells had the opposite effect. Our coIP data suggest that CDYL2 might regulate G9a levels at *MIR124* genes via a mechanism involving physical association of the two factors, whereas they only weakly support this possibility in the case of EZH2. We speculate that an indirect mechanism could account for the strong effects of CDYL2 over-expression and RNAi on EZH2 enrichment upstream of *MIR124* genes, such as the previously described regulation of EZH2 levels on chromatin by G9a methyltransferase activity (Mozzetta et al., 2014). However, the inhibition of the catalytic activity of EZH2 using the small molecule CPI-169 was not sufficient to de-repress miR-124 expression in MCF7-CDYL2 cells. This indicates that recruitment of the EZH2 methyltransferase activity to MIR124 genes by CDYL2 is not sufficient for their repression. Taken together, our findings are consistent with the idea that CDYL2 regulation of G9a enrichment at *MIR124* genes promotes their transcriptional repression, likely via local increases in H3K9me2. Although CDYL2 also regulated the enrichment of EZH2 and H3K9me3 levels upstream of *MIR124* genes, the weak interaction between CDYL2 and EZH2/SUZ12 and failure of CPI-169 to reverse CDYL2 repression of *MIR124* genes in MCF7 cells suggests that these may be indirect and not sufficient for CDYL2 repression of miR-124.

MIR124 genes are emerging tumor suppressors commonly silenced in various cancers including breast (Conaco et al., 2006; Sullivan et al., 2009, p. 124; Wang et al., 2016a, p. 124; Wang et al., 2016b, p. 124). miR-124-3p directly targets STAT3 mRNA and antagonizes p65/NF-κB by inhibiting multiple components of its signaling pathway. It also regulates EMT, migration, invasion, and stemness (Ji et al., 2019; Lv et al., 2011, p. 124; Wang et al., 2016a, p. 124). Importantly, we showed that CDYL2 over-expression up-regulated the levels of active STAT3 and p65 in MCF7 cells, whereas CDYL2 RNAi down-regulated their levels in MDA-MB-231 cells. These observations were consistent with the effects of CDYL2 gain or loss of function on miR-124 levels, suggesting a functional association. Further supporting this possibility, CDYL2 up-regulation of STAT3 and NF-κB signaling in MCF7 cells was suppressed by a miR-124-3p mimic, whereas CDYL2 RNAi down-regulation of STAT3 and NF-κB signaling was rescued by a miR-124-3p inhibitor. Our data suggest that CDYL2 might regulate STAT3 levels via direct targeting by miR-124-3p, as the levels of total STAT3 were increased or diminished in accordance with CDYL2 gain or loss of function. Owing to the diversity of miR-124-3p targets implicated in NF-κB regulation across different cell types, it is challenging to determine which ones might connect CDYL2 with NF-κB regulation. Based on our studies, candidates include BIRC3, RELA, and STAT3 in MCF7 cells, all of which were up-regulated upon CDYL2 over-expression and are known to link miR-124 with NF-κB regulation (Cao et al., 2018, p. 3; Mehta et al., 2017; Wang et al., 2016a). In MDA-MB-231 cells, they include RELA and STAT3, which were down-regulated upon CDYL2 RNAi.

In accordance with the known effects of constitutive NF-κB and STAT3 signaling in cancer cells (Banerjee and Resat, 2016; Huber et al., 2004, p.; Wu et al., 2009), stable over-expression of CDYL2 induced migration and invasiveness in MCF7 cells *in vitro*. Likewise, whereas control MCF7 cells injected into zebrafish embryos seldom metastasized, cells over-expressing CDYL2 frequently did so. In complementary experiments, we showed that CDYL2 RNAi suppressed migration and invasion of MDA-MB-231 cells, which are normally highly invasive. CDYL2 RNAi also diminished the metastatic potential of MDA-MB-231 cells

injected into zebrafish embryos. NF-κB and STAT3 signaling also promote the emergence of breast cancer stem cells, which are believed to play crucial roles in malignant progression (Marotta et al., 2011; Shostak and Chariot, 2011; Wang et al., 2016a; Zhou et al., 2008). We showed that CDYL2 over-expression augmented mammosphere formation in MCF7 cells, suggesting an increase in the proportion of stem-like cells in the culture. Consistent with this, we also observed an increase in the proportion of cells expressing the breast cancer stem cell marker profile CD44-high/CD24-low. In complementary assays, CDYL2 RNAi in MDA-MB-231 cells decreased both mammosphere formation and the fraction of CD44-high/CD24-low cells. These findings support the notion that CDYL2 not only promotes breast cancer cell migration and invasion but also stemness. As was the case for invasion, CDYL2 induction of both invasiveness and mammosphere formation was suppressed by RNAi knockdown of either NF-κB or STAT3, indicating key roles of these pathways in CDYL2 regulation of cancer cell biology.

It has been proposed that in certain malignancies, including breast, molecular and cellular changes that promote the emergence of mesenchymal-like cells constitute a key enabling step in the process of malignant progression (Huber et al., 2004; Puisieux et al., 2014; Sarrio et al., 2008; Shibue and Weinberg, 2017). We found that stable over-expression of CDYL2 induced morphological and molecular changes in the normally non-invasive, epithelioid, MCF7 cells, strongly indicative of an EMT. While transient transfection of MDA-MB-231 cells with siRNA targeting CDYL2 altered the expression of some genes consistent with a partial loss of mesenchymal cell identity, and impaired invasiveness and mammospheres formation in these cells, it did not induce any striking morphological changes. This is consistent with a partial reversal of the EMT state. However, when CDYL2 was knocked down for a longer duration using lentiviral RNAi vectors, we observed clusters of cells forming epithelial-like cobblestone monolayers after 2 to 3 weeks, suggesting a more advanced EMT reversal. These cells also exhibited down-regulation of several EMT-related genes (*LCN2, CTGF, FOSB, JUNB,* and *MYC*) that were over-expressed in MCF7-CDYL2 cells but not down-regulated by transient knock-down of CDYL2 in MDA-MB-231. This difference in gene expression may account for the observation of changes in cell morphology only after prolonged CDYL2 knock-down. In genetic suppression experiments, we found that the EMT-like gene expression program activated in MCF7-CDYL2 cells was antagonized by RNAi knock-down of either STAT3 or p65. These data argue that CDYL2 induction of migration, invasion, metastasis, and stemness in breast cancer cells might be due in part to its regulation of EMT states via up-regulation of NF-κB and STAT3 signaling.

Overall, our studies are consistent with an oncogenic effect of CDYL2 over-expression in breast cancer. This might contribute to the poor prognosis of the patients with ER+/HER2− and TN breast cancer whose cancers express high levels of CDYL2. Although not studied in depth here, we also observed a correlation between high CDYL2 expression and poor prognosis in lung and colorectal carcinomas, hinting at a wider role in cancer. Given the emergence of epigenetic factors as viable therapeutic targets in cancer, our study supports the further evaluation of CDYL2 as a candidate drug target in breast cancer, and potentially other malignancies.

Limitations of the Study

Our study provides several lines of molecular and cellular evidence supporting roles for CDYL2 in regulating EMT, stemness, and cancer cell migration and invasion. Future studies should further extend these findings using murine models of breast cancer cell growth, invasion, and stemness. Although we showed that both G9a and EZH2 were involved in the mechanism of CDYL2 regulation of *MIR124* genes, several molecular details remain to be fully elucidated. For instance, given the weak coIP between CDYL2 and EZH2, it remains to be determined how over-expression or knock-down of CDYL2 exerts comparably strong effects on EZH2 chromatin levels at *MIR124* genes. We speculate that this may be due to the previously described ability of G9a to regulate EZH2 enrichment at certain chromatin loci in a manner that depends on an intact G9a histone methyltransferase activity (Mozzetta et al., 2014), but this remains to be demonstrated in our models. An important aspect of this study is that it links the previously uncharacterized CDYL2 with pathways and genes of established importance in breast cancer, notably *MIR124* genes and signaling via the STAT3 and NF-κB pathways. However, we do not exclude the possibility that CDYL2 regulation of other genes and pathways may also contribute to the cellular phenotypes we observed, and the role of CDYL2 in cancer.

Resource Availability

Lead Contact

Further information and requests for resources and reagents should be directed to and will be fulfilled by the Lead Contact, Peter Mulligan (peter.mulligan@inserm.fr).

Materials Availability

All unique/stable reagents generated in this study are available from the Lead Contact with a completed Materials Transfer Agreement.

Data and Code Availability

The published article includes all datasets generated or analyzed during this study. They are also available via NCBI GEO: GSE150320.

METHODS

All methods can be found in the accompanying Transparent Methods supplemental file.

SUPPLEMENTAL INFORMATION

Supplemental Information can be found online at https://doi.org/10.1016/j.isci.2020.101141.

ACKNOWLEDGMENTS

We gratefully acknowledge the technical assistance provided by Aurelie Jullien and Valery Attignon. We thank Christophe Ginestier, Toufic Renno, and Hichem Mertani for helpful technical discussions and sharing of protocols. This work was funded by grant number PLBIO2016-180 from l'Institut National du Cancer, grant number AJE20131128936 from La Fondation pour la recherche médicale, and financial support from le Centre Léon Bérard, and l'Institut national de la santé et de la recherche médicale, France (Inserm).

AUTHOR CONTRIBUTIONS

M.S.: execution and analysis of majority of experiments; writing of original and updated manuscript; supervision and mentorship of other project participants; co-ordination with other co-authors. P.M.: conceptualization, funding acquisition, project administration, supervision and mentorship of other project members, investigation, formal analysis, writing of original and updated manuscript. P.S. and H.G.: conceptualization, project administration, funding acquisition, formal analysis; M.A.M.-P.: formal analysis; A.D.D.: investigation; L.B.B.: investigation; M.O.: conceptualization, investigation; G.I.: conceptualization and investigation; L.T., A.V., M.R., J.-P.F., V.L., S.N.M., A.P., J.B., and B.G.: formal analysis.

DECLARATION OF INTERESTS

The authors have no conflicts of interest to declare.

Received: December 20, 2019
Revised: March 31, 2020
Accepted: May 4, 2020
Published: June 26, 2020

REFERENCES

Alam, M., Rajabi, H., Ahmad, R., Jin, C., and Kufe, D. (2014). Targeting the MUC1-C oncoprotein inhibits self-renewal capacity of breast cancer cells. Oncotarget *5*, 2622–2634.

Bakiri, L., Macho-Maschler, S., Custic, I., Niemiec, J., Guio-Carrion, A., Hasenfuss, S.C., Eger, A., Muller, M., Beug, H., and Wagner, E.F. (2015). Fra-1/AP-1 induces EMT in mammary epithelial cells by modulating Zeb1/2 and TGFbeta expression. Cell Death Differ. *22*, 336–350.

Banerjee, K., and Resat, H. (2016). Constitutive activation of STAT3 in breast cancer cells: a review. Int. J. Cancer *138*, 2570–2578.

Bradley, W.D., Arora, S., Busby, J., Balasubramanian, S., Gehling, V.S., Nasveschuk, C.G., Vaswani, R.G., Yuan, C.-C., Hatton, C., Zhao, F., et al. (2014). EZH2 inhibitor efficacy in non-Hodgkin's lymphoma does not require suppression of H3K27 monomethylation. Chem. Biol. *21*, 1463–1475.

Cancer Genome Atlas Network (2012). Comprehensive molecular portraits of human breast tumours. Nature *490*, 61–70.

Cao, J., Qiu, J., Wang, X., Lu, Z., Wang, D., Feng, H., Li, X., Liu, Q., Pan, H., and Han, X. (2018). Identification of microRNA-124 in regulation of Hepatocellular carcinoma through BIRC3 and the NF-κB pathway. J. Cancer *9*, 3006.

Chang, C.-J., Yang, J.-Y., Xia, W., Chen, C.-T., Xie, X., Chao, C.-H., Woodward, W.A., Hsu, J.-M., Hortobagyi, G.N., and Hung, M.-C. (2011). EZH2 promotes expansion of breast tumor initiating cells through activation of RAF1-β-catenin signaling. Cancer Cell *19*, 86–100.

Chen, D.-T., Nasir, A., Culhane, A., Venkataramu, C., Fulp, W., Rubio, R., Wang, T., Agrawal, D., McCarthy, S.M., Gruidl, M., et al. (2010). Proliferative genes dominate malignancy-risk gene signature in histologically-normal breast tissue. Breast Cancer Res. Treat. *119*, 335–346.

Conaco, C., Otto, S., Han, J.-J., and Mandel, G. (2006). Reciprocal actions of REST and a microRNA promote neuronal identity. PNAS *103*, 2422–2427.

Curry, E., Green, I., Chapman-Rothe, N., Shamsaei, E., Kandil, S., Cherblanc, F.L., Payne, L., Bell, E., Ganesh, T.,

Srimongkolpithak, N., et al. (2015). Dual EZH2 and EHMT2 histone methyltransferase inhibition increases biological efficacy in breast cancer cells. Clin. Epigenetics *7*, 84.

Dawson, M.A., and Kouzarides, T. (2012). Cancer epigenetics: from mechanism to therapy. Cell *150*, 12–27.

Dhasarathy, A., Kajita, M., and Wade, P.A. (2007). The transcription factor snail mediates epithelial to mesenchymal transitions by repression of estrogen receptor-α. Mol. Endocrinol. *21*, 2907–2918.

Dong, C., Wu, Y., Yao, J., Wang, Y., Yu, Y., Rychahou, P.G., Evers, B.M., and Zhou, B.P. (2012). G9a interacts with Snail and is critical for Snail-mediated E-cadherin repression in human breast cancer. J. Clin. Invest. *122*, 1469–1486.

Dorus, S., Gilbert, S.L., Forster, M.L., Barndt, R.J., and Lahn, B.T. (2003). The CDY-related gene family: coordinated evolution in copy number, expression profile and protein sequence. Hum. Mol. Genet. *12*, 1643–1650.

Ellis, M.J., Gillette, M., Carr, S.A., Paulovich, A.G., Smith, R.D., Rodland, K.K., Townsend, R.R., Kinsinger, C., Mesri, M., Rodriguez, H., and Liebler, D.C.; Clinical Proteomic Tumor Analysis Consortium (CPTAC) (2013). Connecting genomic alterations to cancer biology with proteomics: the NCI clinical proteomic tumor analysis Consortium. Cancer Discov. *3*, 1108–1112.

Fischle, W., Franz, H., Jacobs, S.A., Allis, C.D., and Khorasanizadeh, S. (2008). Specificity of the chromodomain Y chromosome family of chromodomains for lysine-methylated ARK(S/T) motifs. J. Biol. Chem. *283*, 19626–19635.

Franz, H., Mosch, K., Soeroes, S., Urlaub, H., and Fischle, W. (2009). Multimerization and H3K9me3 binding are required for CDYL1b heterochromatin association. J. Biol. Chem. *284*, 35049–35059.

Gatti, V., Bongiorno-Borbone, L., Fierro, C., Annicchiarico-Petruzzelli, M., Melino, G., and Peschiaroli, A. (2019). p63 at the crossroads between stemness and metastasis in breast cancer. Int. J. Mol. Sci. *20*, 2683.

Hatziapostolou, M., Polytarchou, C., Aggelidou, E., Drakaki, A., Poultsides, G.A., Jaeger, S.A., Ogata, H., Karin, M., Struhl, K., Hadzopoulou-Cladaras, M., and Iliopoulos, D. (2011). An HNF4α-miRNA inflammatory feedback circuit regulates hepatocellular oncogenesis. Cell *147*, 1233–1247.

Huber, M.A., Azoitei, N., Baumann, B., Grunert, S., Sommer, A., Pehamberger, H., Kraut, N., Beug, H., and Wirth, T. (2004). NF-kappaB is essential for epithelial-mesenchymal transition and metastasis in a model of breast cancer progression. J. Clin. Invest. *114*, 569–581.

Jambhekar, A., Dhall, A., and Shi, Y. (2019). Roles and regulation of histone methylation in animal development. Nat. Rev. Mol. Cell Biol. *1*, https://doi.org/10.1038/s41580-019-0151-1.

Ji, H., Sang, M., Liu, F., Ai, N., and Geng, C. (2019). miR-124 regulates EMT based on ZEB2 target to inhibit invasion and metastasis in triple-negative breast cancer. Pathol. Res. Pract. *215*, 697–704.

Jiao, X., Katiyar, S., Willmarth, N.E., Liu, M., Ma, X., Flomenberg, N., Lisanti, M.P., and Pestell, R.G. (2010). c-Jun induces mammary epithelial cellular invasion and breast cancer stem cell expansion. J. Biol. Chem. *285*, 8218–8226.

Kim, G., Ouzounova, M., Quraishi, A.A., Davis, A., Tawakkol, N., Clouthier, S.G., Malik, F., Paulson, A.K., D'Angelo, R.C., Korkaya, S., et al. (2015). SOCS3-mediated regulation of inflammatory cytokines in PTEN and p53 inactivated triple negative breast cancer model. Oncogene *34*, 671–680.

Kim, Y., Lee, H.-M., Xiong, Y., Sciaky, N., Hulbert, S.W., Cao, X., Everitt, J.I., Jin, J., Roth, B.L., and Jiang, Y.-H. (2017). Targeting the histone methyltransferase G9a activates imprinted genes and improves survival of a mouse model of Prader-Willi syndrome. Nat. Med. *23*, 213–222.

Kretschmer, C., Sterner-Kock, A., Siedentopf, F., Schoenegg, W., Schlag, P.M., and Kemmner, W. (2011). Identification of early molecular markers for breast cancer. Mol. Cancer *10*, 15.

Kufe, D.W. (2013). MUC1-C oncoprotein as a target in breast cancer: activation of signaling pathways and therapeutic approaches. Oncogene *32*, 1073–1081.

Lin, Y.-C., Lee, Y.-C., Li, L.-H., Cheng, C.-J., and Yang, R.-B. (2014). Tumor suppressor SCUBE2 inhibits breast-cancer cell migration and invasion through the reversal of epithelial-mesenchymal transition. J. Cell. Sci. *127*, 85–100.

Lv, X.-B., Jiao, Y., Qing, Y., Hu, H., Cui, X., Lin, T., Song, E., and Yu, F. (2011). miR-124 suppresses multiple steps of breast cancer metastasis by targeting a cohort of pro-metastatic genes in vitro. Chin. J. Cancer *30*, 821.

Marotta, L.L., Almendro, V., Marusyk, A., Shipitsin, M., Schemme, J., Walker, S.R., Bloushtain-Qimron, N., Kim, J.J., Choudhury, S.A., and Maruyama, R. (2011). The JAK2/STAT3 signaling pathway is required for growth of CD44+ CD24–stem cell–like breast cancer cells in human tumors. J. Clin. Invest. *121*, 2723–2735.

Mehta, A.K., Hua, K., Whipple, W., Nguyen, M.-T., Liu, C.-T., Haybaeck, J., Weidhaas, J., Settleman, J., and Singh, A. (2017). Regulation of autophagy, NF-κB signaling, and cell viability by miR-124 in KRAS mutant mesenchymal-like NSCLC cells. Sci. Signal. *10*, eaam6291.

Michailidou, K., Hall, P., Gonzalez-Neira, A., Ghoussaini, M., Dennis, J., Milne, R.L., Schmidt, M.K., Chang-Claude, J., Bojesen, S.E., Bolla, M.K., et al. (2013). Large-scale genotyping identifies 41 new loci associated with breast cancer risk. Nat. Genet. *45*, 353–361, 361.e1-e2.

Mozzetta, C., Pontis, J., Fritsch, L., Robin, P., Portoso, M., Proux, C., Margueron, R., and Ait-Si-Ali, S. (2014). The histone H3 lysine 9 methyltransferases G9a and GLP regulate polycomb repressive complex 2-mediated gene silencing. Mol. Cell *53*, 277–289.

Mulligan, P., Westbrook, T.F., Ottinger, M., Pavlova, N., Chang, B., Macia, E., Shi, Y.J., Barretina, J., Liu, J., Howley, P.M., et al. (2008). CDYL bridges REST and histone methyltransferases for gene repression and suppression of cellular transformation. Mol. Cell *32*, 718–726.

Nair, R., Roden, D.L., Teo, W.S., McFarland, A., Junankar, S., Ye, S., Nguyen, A., Yang, J., Nikolic, I., Hui, M., et al. (2014). c-Myc and Her2 cooperate to drive a stem-like phenotype with poor prognosis in breast cancer. Oncogene *33*, 3992–4002.

Olarerin-George, A.O., Anton, L., Hwang, Y.-C., Elovitz, M.A., and Hogenesch, J.B. (2013). A functional genomics screen for microRNA regulators of NF-kappaB signaling. BMC Biol. *11*, 19.

Piva, M., Domenici, G., Iriondo, O., Rabano, M., Simoes, B.M., Comaills, V., Barredo, I., Lopez-Ruiz, J.A., Zabalza, I., Kypta, R., and Vivanco, M. (2014). Sox2 promotes tamoxifen resistance in breast cancer cells. EMBO Mol. Med. *6*, 66–79.

Puisieux, A., Brabletz, T., and Caramel, J. (2014). Oncogenic roles of EMT-inducing transcription factors. Nat. Cell Biol. *16*, 488–494.

Rhodes, D.R., Yu, J., Shanker, K., Deshpande, N., Varambally, R., Ghosh, D., Barrette, T., Pandey, A., and Chinnaiyan, A.M. (2004). ONCOMINE: a cancer microarray database and integrated data-mining platform. Neoplasia *6*, 1–6.

Rizki, A., Weaver, V.M., Lee, S.-Y., Rozenberg, G.I., Chin, K., Myers, C.A., Bascom, J.L., Mott, J.D., Semeiks, J.R., Grate, L.R., et al. (2008). A human breast cell model of preinvasive to invasive transition. Cancer Res. *68*, 1378–1387.

Romagnoli, M., Belguise, K., Yu, Z., Wang, X., Landesman-Bollag, E., Seldin, D.C., Chalbos, D., Barille-Nion, S., Jezequel, P., Seldin, M.L., and Sonenshein, G.E. (2012). Epithelial-to-mesenchymal transition induced by TGF-beta1 is mediated by Blimp-1-dependent repression of BMP-5. Cancer Res. *72*, 6268–6278.

Sarrio, D., Rodriguez-Pinilla, S.M., Hardisson, D., Cano, A., Moreno-Bueno, G., and Palacios, J. (2008). Epithelial-mesenchymal transition in breast cancer relates to the basal-like phenotype. Cancer Res. *68*, 989–997.

Shibue, T., and Weinberg, R.A. (2017). EMT, CSCs, and drug resistance: the mechanistic link and clinical implications. Nat. Rev. Clin. Oncol. *14*, 611–629.

Shimo, T., Kubota, S., Yoshioka, N., Ibaragi, S., Isowa, S., Eguchi, T., Sasaki, A., and Takigawa, M. (2006). Pathogenic role of connective tissue growth factor (CTGF/CCN2) in osteolytic metastasis of breast cancer. J. Bone Miner Res. *21*, 1045–1059.

Shostak, K., and Chariot, A. (2011). NF-kappaB, stem cells and breast cancer: the links get stronger. Breast Cancer Res. *13*, 214.

Simó-Riudalbas, L., and Esteller, M. (2015). Targeting the histone orthography of cancer: drugs for writers, erasers and readers. Br. J. Pharmacol. *172*, 2716–2732.

Singh, J.K., Simoes, B.M., Howell, S.J., Farnie, G., and Clarke, R.B. (2013). Recent advances reveal IL-8 signaling as a potential key to targeting breast cancer stem cells. Breast Cancer Res. *15*, 210.

Subramanian, A., Tamayo, P., Mootha, V.K., Mukherjee, S., Ebert, B.L., Gillette, M.A.,

Paulovich, A., Pomeroy, S.L., Golub, T.R., Lander, E.S., and Mesirov, J.P. (2005). Gene set enrichment analysis: a knowledge-based approach for interpreting genome-wide expression profiles. Proc. Natl. Acad. Sci. U S A *102*, 15545–15550.

Sullivan, N.J., Sasser, A.K., Axel, A.E., Vesuna, F., Raman, V., Ramirez, N., Oberyszyn, T.M., and Hall, B.M. (2009). Interleukin-6 induces an epithelial-mesenchymal transition phenotype in human breast cancer cells. Oncogene *28*, 2940–2947.

Tachibana, M., Ueda, J., Fukuda, M., Takeda, N., Ohta, T., Iwanari, H., Sakihama, T., Kodama, T., Hamakubo, T., and Shinkai, Y. (2005). Histone methyltransferases G9a and GLP form heteromeric complexes and are both crucial for methylation of euchromatin at H3-K9. Genes Dev. *19*, 815–826.

Wang, X., Li, Y., Dai, Y., Liu, Q., Ning, S., Liu, J., Shen, Z., Zhu, D., Jiang, F., Zhang, J., and Li, Z. (2016a). Sulforaphane improves chemotherapy efficacy by targeting cancer stem cell-like properties via the miR-124/IL-6R/STAT3 axis. Sci. Rep. *6*, 36796.

Wang, Y., Chen, L., Wu, Z., Wang, M., Jin, F., Wang, N., Hu, X., Liu, Z., Zhang, C.-Y., Zen, K., et al. (2016b). miR-124-3p functions as a tumor suppressor in breast cancer by targeting CBL. BMC Cancer *16*, 826.

Wu, H., Zhang, H., Wang, P., Mao, Z., Feng, L., Wang, Y., Liu, C., Xia, Q., Li, B., Zhao, H., et al. (2013). Short-Form CDYLb but not long-form CDYLa functions cooperatively with histone methyltransferase G9a in hepatocellular carcinomas. Genes Chromosomes Cancer *52*, 644–655.

Wu, Y., Deng, J., Rychahou, P.G., Qiu, S., Evers, B.M., and Zhou, B.P. (2009). Stabilization of snail by NF-kappaB is required for inflammation-induced cell migration and invasion. Cancer cell *15*, 416–428.

Yang, L., Han, S., and Sun, Y. (2014). An IL6-STAT3 loop mediates resistance to PI3K inhibitors by inducing epithelial-mesenchymal transition and cancer stem cell expansion in human breast cancer cells. Biochem. Biophys. Res. Commun. *453*, 582–587.

Yin, L., Castagnino, P., and Assoian, R.K. (2008). ABCG2 expression and side population abundance regulated by a transforming growth factor beta-directed epithelial-mesenchymal transition. Cancer Res. *68*, 800–807.

Yu, F., Li, J., Chen, H., Fu, J., Ray, S., Huang, S., Zheng, H., and Ai, W. (2011). Kruppel-like factor 4 (KLF4) is required for maintenance of breast cancer stem cells and for cell migration and invasion. Oncogene *30*, 2161–2172.

Zhang, Y., Yang, X., Gui, B., Xie, G., Zhang, D., Shang, Y., and Liang, J. (2011). Corepressor protein CDYL functions as a molecular bridge between polycomb repressor complex 2 and repressive chromatin mark trimethylated histone lysine 27. J. Biol. Chem. *286*, 42414–42425.

Zhou, H., Tang, K., Liu, H., Zeng, J., Li, H., Yan, L., Hu, J., Guan, W., Chen, K., and Xu, H. (2019). Regulatory Network of two tumor-suppressive noncoding RNAs interferes with the growth and metastasis of renal cell carcinoma. Mol. Ther. Nucleic Acids *16*, 554–565.

Zhou, J., Zhang, H., Gu, P., Bai, J., Margolick, J.B., and Zhang, Y. (2008). NF-kappaB pathway inhibitors preferentially inhibit breast cancer stem-like cells. Breast Cancer Res. Treat. *111*, 419–427.

iScience, Volume *23*

Supplemental Information

CDYL2 Epigenetically Regulates *MIR124* to Control NF-κB/STAT3-Dependent Breast Cancer Cell Plasticity

Maha Siouda, Audrey D. Dujardin, Laetitia Barbollat-Boutrand, Marco A. Mendoza-Parra, Benjamin Gibert, Maria Ouzounova, Jebrane Bouaoud, Laurie Tonon, Marie Robert, Jean-Philippe Foy, Vincent Lavergne, Serge N. Manie, Alain Viari, Alain Puisieux, Gabriel Ichim, Hinrich Gronemeyer, Pierre Saintigny, and Peter Mulligan

Supplemental Information:

Supplemental Figure Legends:

Figure S1: CDYL2 expression level is upregulated in a variety of human cancer and is associated with poor prognosis. Related to Figure 1.

(A) Oncomine analysis of cancer cohorts revealed upregulation of CDYL2 mRNA in breast, colorectal, esophagus cancers and leukaemia, but a downregulation in lymphoma.

(B,C) CDYL2 mRNA **(B)** and protein **(C)** expression in the indicated breast cancer sub-types, as derived from analysis of the TCGA and CPTAC breast cancer cohorts. P-values were calculated by t-test. NS: not significant.

(D-F) Expression of CDYL2 in normal breast tissues over or breast cancer at the indicated AJCC stages (pN0 – pN3) across all TCGA breast samples **(D)** or in the ER+/HER2- **(E)** and TN **(F)** sub-types. P-values were calculated by t-test. * $P < 0.05$; ** $P < 0.01$; *** $P < 0.001$; **** $P < 0.0001$.

(G,H) Analysis of the correlation between CDYL2 expression in both ER+/HER2- **(G)** and TN breast cancer **(H)** and the 'Rizki_tumor_invasiveness-2D-UP' GSEA signature.

(I,J) Kaplan–Meier overall survival (OS) analysis performed from TCGA colorectal cancer **(I)**, or rectal adenocarcinoma **(J)**. High or low CDYL2 mRNA was based best cut-off. Significance using LogRank p-value and Hazard Ratio (CI) are indicated.

(K,L) Kaplan–Meier overall survival (OS) analysis performed from TCGA lung squamous cell carcinoma **(K)** or lung adenocarcinoma **(L)**. High or low CDYL2 mRNA was based respectively on best cut-off of and highest versus lowest quartiles. Significance using LogRank p-value and Hazard Ratio (CI) are indicated.

Figure S1

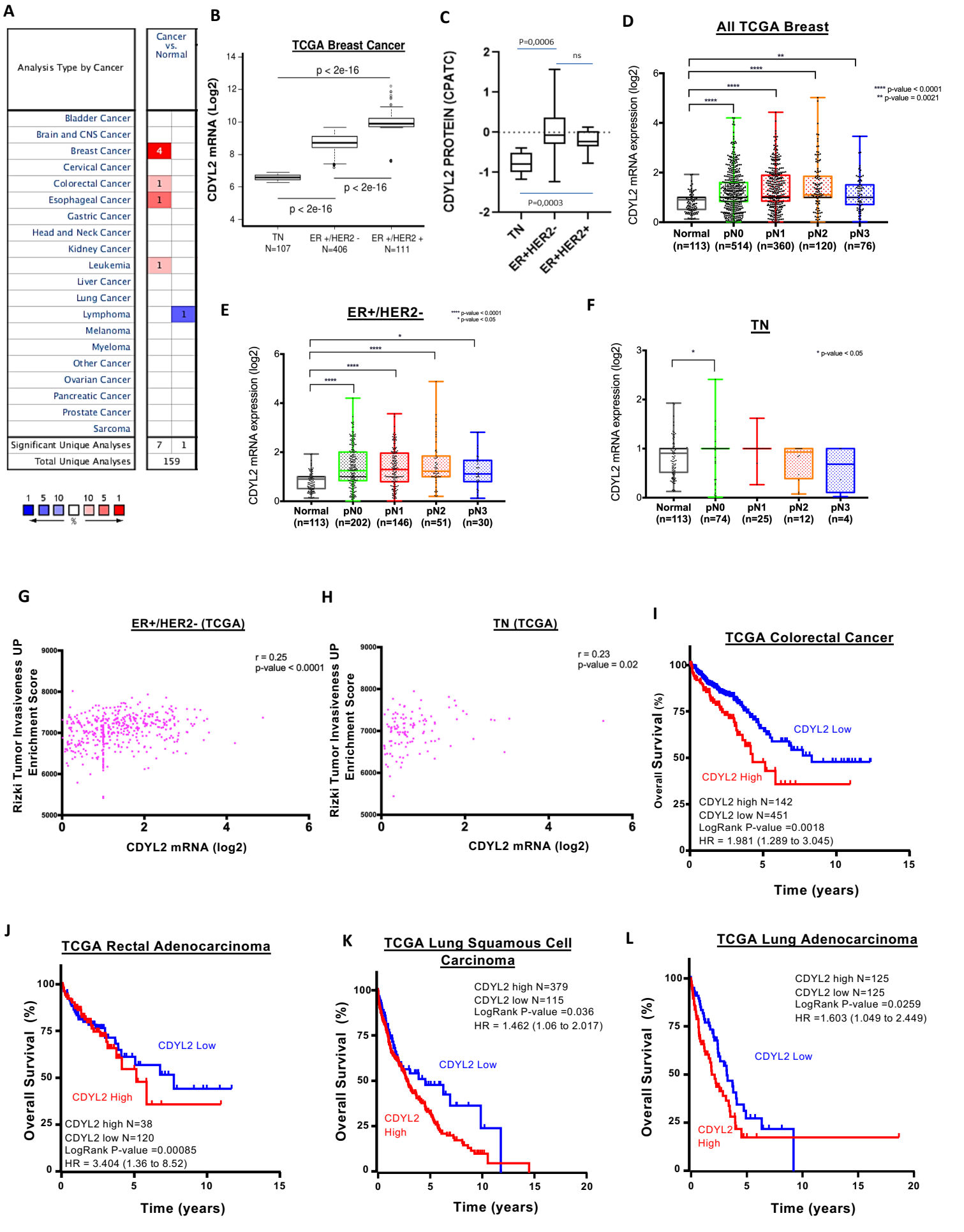
A
Analysis Type by Cancer
Cancer vs. Normal
Bladder Cancer
Brain and CNS Cancer
Breast Cancer
Cervical Cancer
Colorectal Cancer
Esophageal Cancer
Gastric Cancer
Head and Neck Cancer
Kidney Cancer
Leukemia
Liver Cancer
Lung Cancer
Lymphoma
Melanoma
Myeloma
Other Cancer
Ovarian Cancer
Pancreatic Cancer
Prostate Cancer
Sarcoma
Significant Unique Analyses
Total Unique Analyses
B
TCGA Breast Cancer
CDYL2 mRNA (Log2)
p < 2e-16
TN N=107
ER +/HER2 - N=406
ER +/HER2 + N=111
C
CDYL2 PROTEIN (CPATC)
P=0,0006
ns
P=0,0003
TN
ER+HER2-
ER+HER2+
D
All TCGA Breast
CDYL2 mRNA expression (log2)
**** p-value < 0.0001
** p-value = 0.0021
Normal (n=113)
pN0 (n=514)
pN1 (n=360)
pN2 (n=120)
pN3 (n=76)
E
ER+/HER2-
**** p-value < 0.0001
* p-value < 0.05
Normal (n=113)
pN0 (n=202)
pN1 (n=146)
pN2 (n=51)
pN3 (n=30)
F
TN
* p-value < 0.05
Normal (n=113)
pN0 (n=74)
pN1 (n=25)
pN2 (n=12)
pN3 (n=4)
G
ER+/HER2- (TCGA)
Rizki Tumor Invasiveness UP Enrichment Score
r = 0.25
p-value < 0.0001
CDYL2 mRNA (log2)
H
TN (TCGA)
Rizki Tumor Invasiveness UP Enrichment Score
r = 0.23
p-value = 0.02
CDYL2 mRNA (log2)
I
TCGA Colorectal Cancer
Overall Survival (%)
CDYL2 Low
CDYL2 High
CDYL2 high N=142
CDYL2 low N=451
LogRank P-value =0.0018
HR = 1.981 (1.289 to 3.045)
Time (years)
J
TCGA Rectal Adenocarcinoma
Overall Survival (%)
CDYL2 Low
CDYL2 High
CDYL2 high N=38
CDYL2 low N=120
LogRank P-value =0.00085
HR = 3.404 (1.36 to 8.52)
Time (years)
K
TCGA Lung Squamous Cell Carcinoma
CDYL2 high N=379
CDYL2 low N=115
LogRank P-value =0.036
HR = 1.462 (1.06 to 2.017)
Overall Survival (%)
CDYL2 Low
CDYL2 High
Time (years)
L
TCGA Lung Adenocarcinoma
CDYL2 high N=125
CDYL2 low N=125
LogRank P-value =0.0259
HR =1.603 (1.049 to 2.449)
Overall Survival (%)
CDYL2 Low
CDYL2 High
Time (years)

Figure S2: Analysis of the effect of CDYL2 over-expression on MCF7 cell growth and the EpCAM/CD49f profile of MCF7-CDYL2, Cama1-CDYL2 and MDA-MB-231 cells treated with CDYL2 siRNA. Related to Figures 3 and 4.

(A) Cell proliferation was monitored for 5 days by live imaging using the *Incucyte Zoom.* Images were taken every 2 hours. Values plotted represent mean±SD of confluency from three experiments.

(B) Colony formation assay of MCF7-CDYL2 or control (MCF7-Vector) that were seeded at low density, grown for 1 week then stained with Crystal Violet. Colonies count and size were quantified using *Fiji* image analysis software. Significance was determined by T-test ($p > 0.05$).

(C) FACS Scatter plots showing the expression of EpCAM and CD49f antigens on the indicated cell lines either expressing an empty vector or CDYL2 over-expression vector (MCF7, Cama-1) or treated with a control or CDYL2 siRNA (MDA-MB-231).

Figure S2

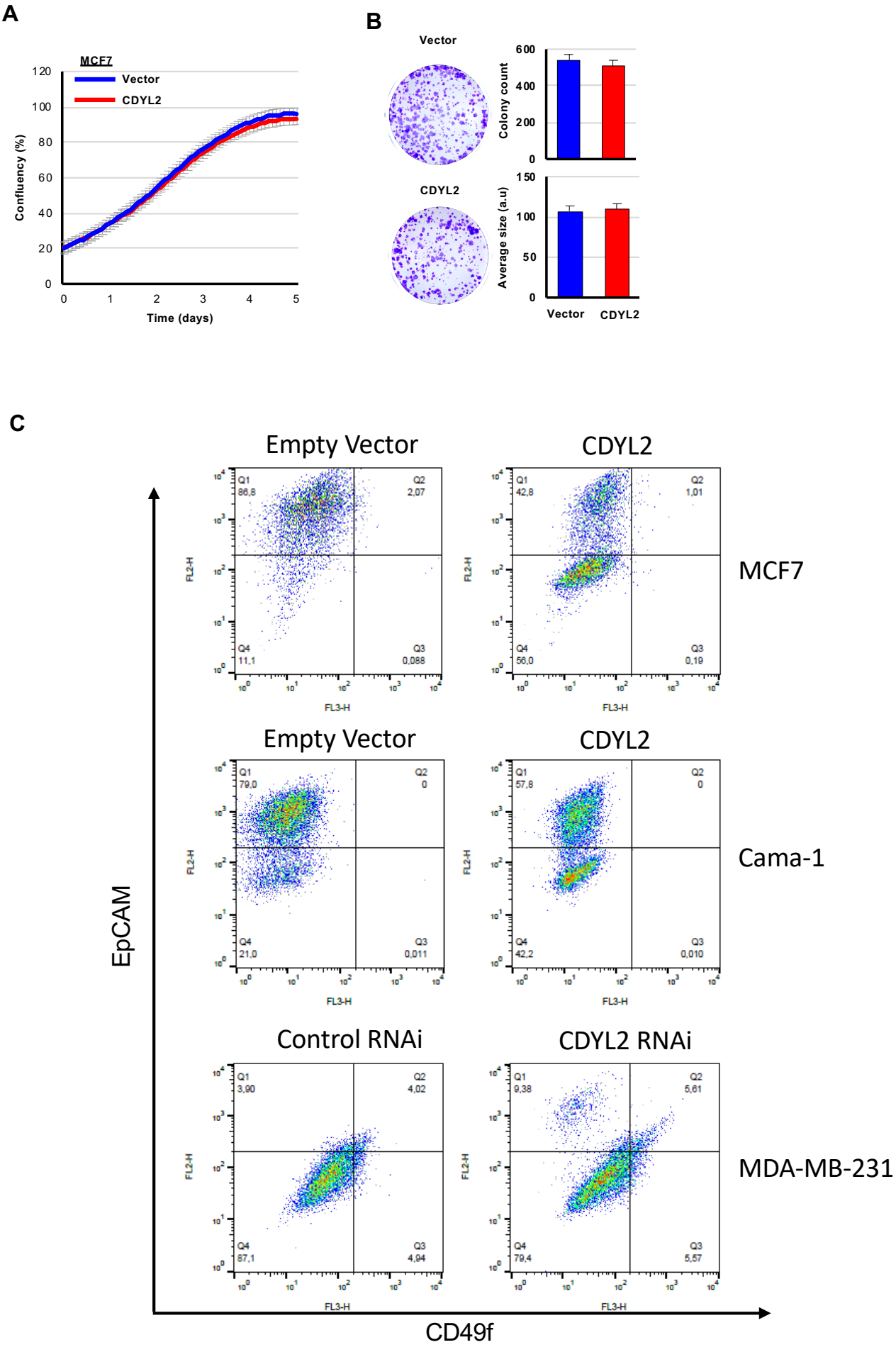
A
MCF7
Vector
CDYL2
Confluency (%)
Time (days)
B
Vector
CDYL2
Colony count
Average size (a.u)
Vector
CDYL2
C
Empty Vector
CDYL2
Control RNAi
CDYL2 RNAi
MCF7
Cama-1
MDA-MB-231
EpCAM
CD49f
FL2-H
FL3-H
Q1 86,8
Q2 2,07
Q4 11,1
Q3 0,088
Q1 42,8
Q2 1,01
Q4 56,0
Q3 0,19
Q1 79,0
Q2 0
Q4 21,0
Q3 0,011
Q1 57,8
Q2 0
Q4 42,2
Q3 0,010
Q1 3,90
Q2 4,02
Q4 87,1
Q3 4,94
Q1 9,38
Q2 5,61
Q4 79,4
Q3 5,57

Figure S3: Stable knockdown of CDYL2 in the invasive breast cancer cell line MDA-MB-231 induces transcriptional and phenotypic changes associated with inhibition of malignancy. Related to Figure 4.

(A) CDYL2 knockdown was confirmed by western blotting as well as protein levels of EMT markers Vimentin (VIM) and fibronectin (FN). Beta-actin was probed as a loading control.

(B) 10X phase contrast micrograph demonstrating morphological differences consistent with mesenchymal to epithelial transition between MDA-MB-231 with stable knock of CDYL2 (sh-CDYL2) compared to control (sh-Ctr). Scale bar, 100 μm.

(C) q-RT PCR validation of selected genes involved in loss of EMT. Values are normalized to GAPDH. Data are represented as mean of three independent experiments ± S.D. Significance was determined by t-test (differences shown were significant at $p < 0.05$).

(D,E) stable CDYL2 sh-RNA in MDA-MB-231 cells decreased the rate of migration across a porous membrane **(D)** and suppressed invasiveness of cells across porous membranes overlaid with Matrigel **(E).** Graphs shown are representative of three independent experiments in quadruple runs per condition.

(F) Mammospheres formation from cells plated at the indicated seeding number per well in 96-well plates, mammospheres with size > 50μm counted after 8 days. Shown is a scatter plot of the results of a representative of three independent experiments indicating the median (black bar), and T-test significance (** $p<0.01$; *** $p<0.001$).

(G) FACS analysis of antigenic profile associated with breast cancer stem cells (CD44+/CD24low/−).

Figure S3

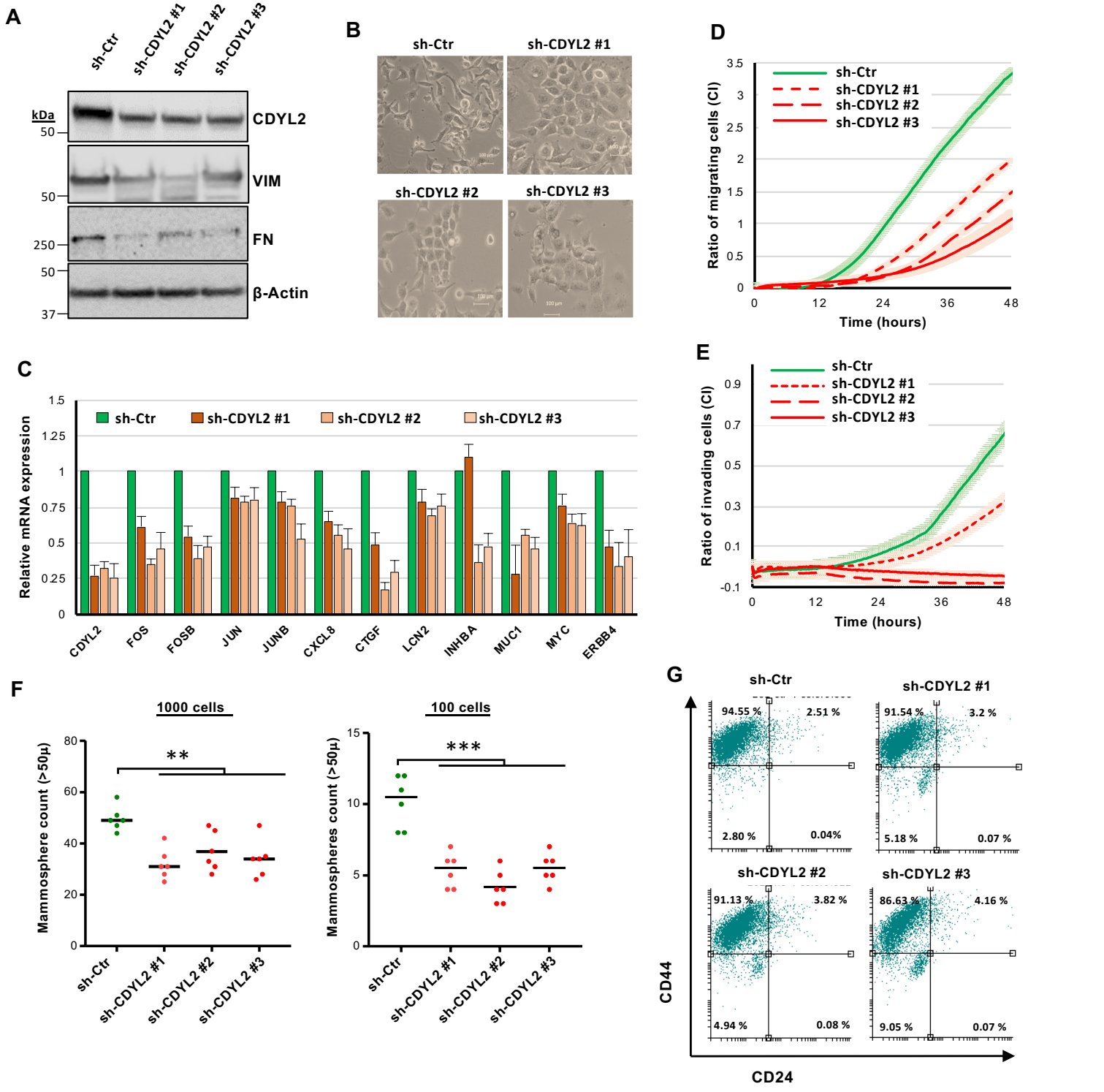
A
sh-Ctr
sh-CDYL2 #1
sh-CDYL2 #2
sh-CDYL2 #3
kDa
50
CDYL2
50
VIM
250
FN
50
β-Actin
37
B
sh-Ctr
sh-CDYL2 #1
sh-CDYL2 #2
sh-CDYL2 #3
D
Ratio of migrating cells (CI)
Time (hours)
sh-Ctr
sh-CDYL2 #1
sh-CDYL2 #2
sh-CDYL2 #3
C
Relative mRNA expression
CDYL2
FOS
FOSB
JUN
JUNB
CXCL8
CTGF
LCN2
INHBA
MUC1
MYC
ERBB4
E
Ratio of invading cells (CI)
Time (hours)
F
1000 cells
100 cells
Mammosphere count (>50µ)
Mammospheres count (>50µ)
**
***
G
CD44
CD24
94.55 %
2.51 %
2.80 %
0.04%
91.54 %
3.2 %
5.18 %
0.07 %
91.13 %
3.82 %
4.94 %
0.08 %
86.63 %
4.16 %
9.05 %
0.07 %

Figure S4: Nuclear localization of CDYL2. Related to Figure 6.

(A) Western blot detection of endogenous CDYL2 in several cellular fractions of MCF7 cells treated with RNAi against CDYL2 (esiCDYL2) or control (esiLuc). Total = whole cell lysate; Cyto.= Cytoplasmic fraction ; N.E. = Soluble nuclear extract ; MX = Matrix, or tight chromatin fraction. **(B,C)** Immunofluorescence detection of CDYL2 (red) in MCF7-Vector and MCF7-CDYL2 cells **(B)** and MDA-MB-231 cells **(C)**. Nuclear DNA is detected by DAPI staining.

Figure S4

A

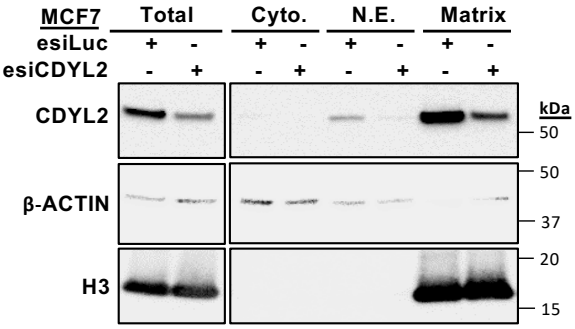

B

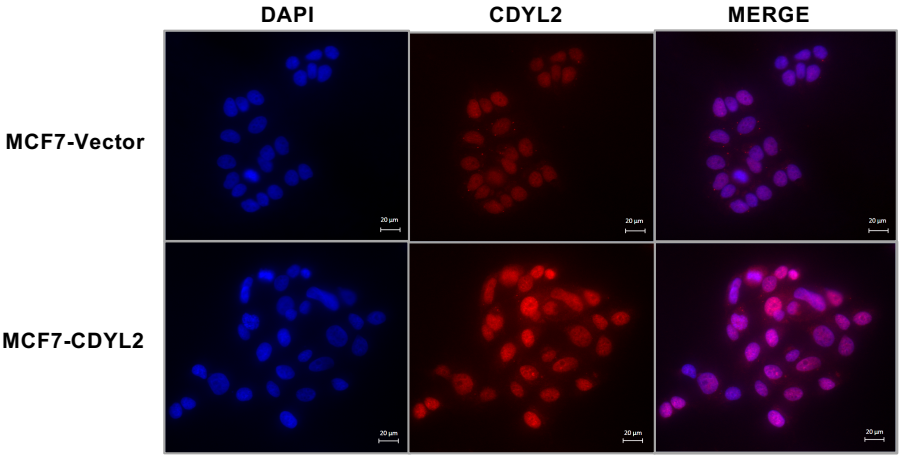

C

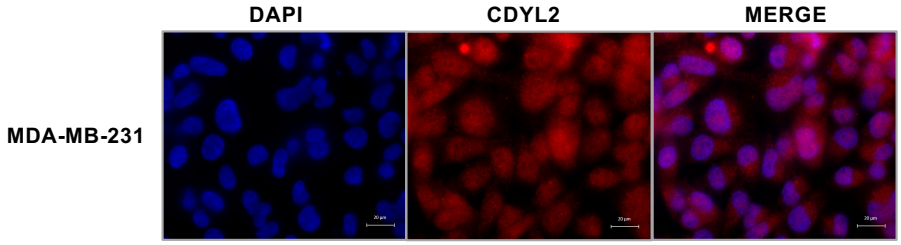

Figure S5: Stable knockdown of CDYL2 in the invasive breast cancer cell line MDA-MB-231 induces increase levels of MIR124. Related to Figure 6.

(A) The expression levels of both the precursor and mature 3' strand of mir-124 were measured by qRT-PCR. Values are the mean +/- S.D. of triplicate experiments. The differences with control are all significant with T-test (*p <0.05).

Figure S5

A

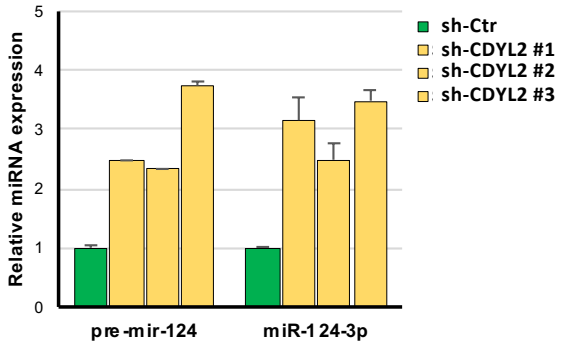
Relative miRNA expression
5
4
3
2
1
0
pre-mir-124
miR-124-3p
sh-Ctr
sh-CDYL2 #1
sh-CDYL2 #2
sh-CDYL2 #3

Figure S6: CDYL2 interacts with the histone methyltransferase G9a and regulates its enrichment and that of EZH2 at the *MIR124* promoter, as well as that of their cognate methylation marks. Related to Figure 7.

(A) Endogenous co-immunoprecipitation of G9a/EHMT2, EZH2 and CDYL2 using their respective endogenous antibodies. The immuno-precipitated proteins were visualized by immunoblotting. Non-specific IgG was used as a control for background binding. H.C.*= IgG Heavy Chain cross-reactivity from the IP antibody.

(B,C) ChIP-qPCR analysis of the enrichment CDYL2, G9a, EZH2, H3K9me2, H3K27me3 at *MIR124-1, MIR124-3* or an additional negative control region (Neg. Ctr. #2) in MCF7-CDYL2 compared to MCF7-Vector **(B)** or MDA-MB-231 treated with esiCDYL2 or esiLuc **(C)**. Enrichment is presented as percentage of Input. Values are the mean +/- S.D. of triplicate experiments. T-test: * $p < 0.05$, ** $p<0.01$; ns= not significant, $p > 0.05$).

Figure S6

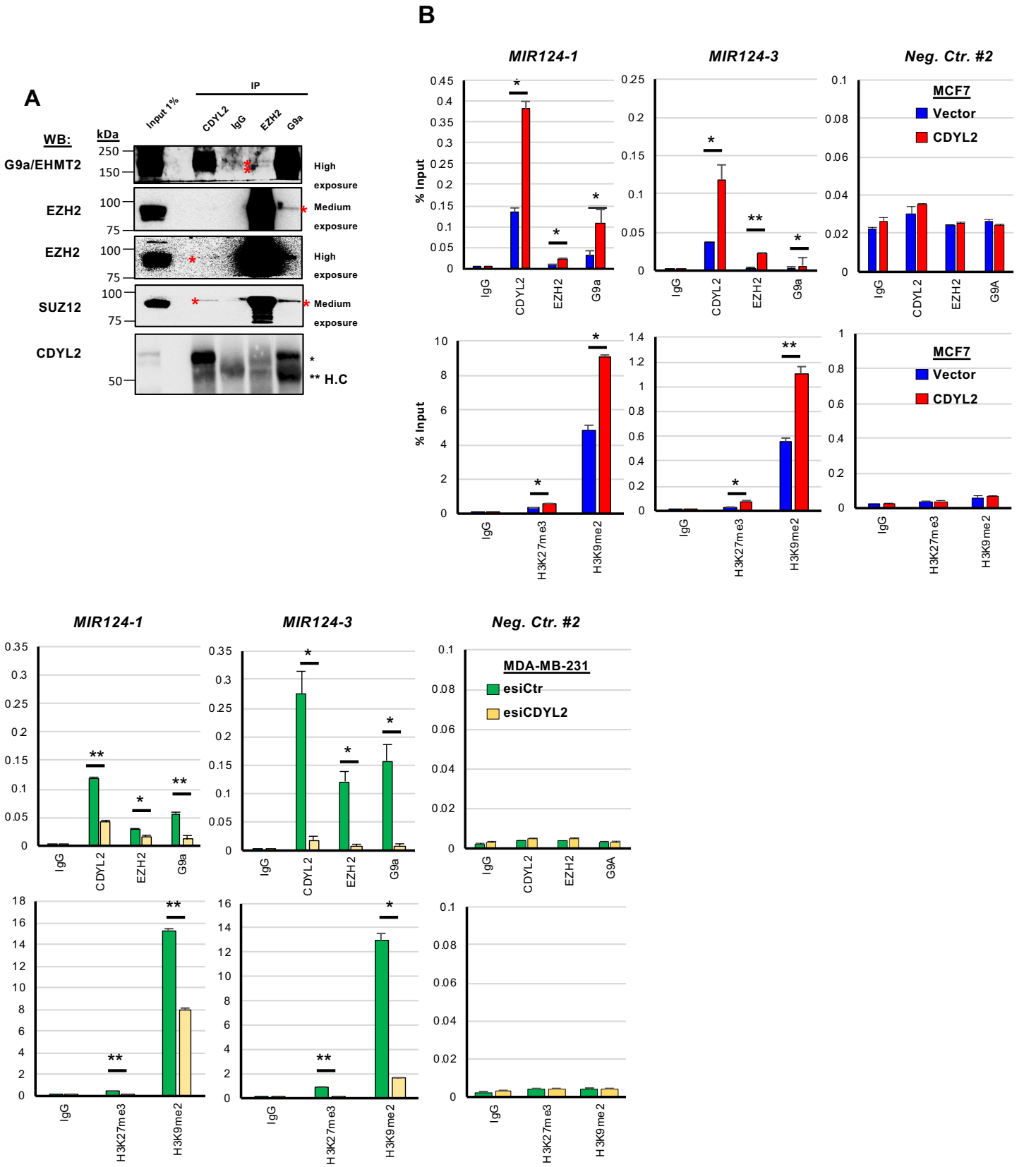
A
IP
Input 1%
CDYL2
IgG
EZH2
G9a
WB:
kDa
G9a/EHMT2
250
150
High exposure
EZH2
100
75
Medium exposure
EZH2
100
75
High exposure
SUZ12
100
75
Medium exposure
CDYL2
50
* H.C
B
MIR124-1
MIR124-3
Neg. Ctr. #2
% Input
MCF7
Vector
CDYL2
IgG
CDYL2
EZH2
G9a
H3K27me3
H3K9me2
C
MIR124-1
MIR124-3
Neg. Ctr. #2
% Input
MDA-MB-231
esiCtr
esiCDYL2
IgG
CDYL2
EZH2
G9a
H3K27me3
H3K9me2

Figure S7: Analysis of the effect of the G9a/GLP inhibitor UNC0642 or the EZH2 inhibitor CPI-169 on miR-124 expression in MCF7-CDYL2 cells. Related to Figure 7.

(A) qRT-PCR analysis of miR-124-3p levels in MCF7-CDYL2 cells treated with 1.1 μM UNC0642 for 24h or 48h. A DMSO vehicle control was included for each time point. Expression was normalized to an unrelated miRNA. Data represent the mean of three independent experiments ± S.D. Significance determined by test, as indicated.

(B) qRT-PCR analysis of miR-124-3p levels in MCF7-CDYL2 cells treated with the indicated concentrations of CPI-169 for 96h. Matching DMSO vehicle controls were included for each concentration of drug used. Expression was normalized to an unrelated miRNA. Data represent the mean of three independent experiments ± S.D. No significant differences were detected by t-test.

Figure S7

A

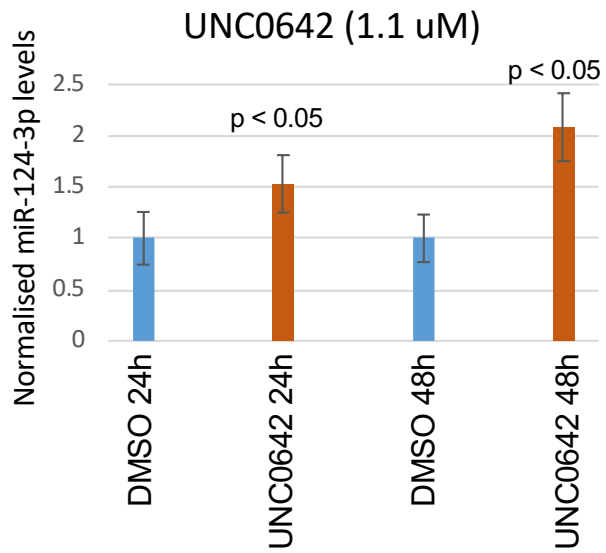
UNC0642 (1.1 uM)
Normalised miR-124-3p levels
2.5
2
1.5
1
0.5
0
p < 0.05
p < 0.05
DMSO 24h
UNC0642 24h
DMSO 48h
UNC0642 48h

B

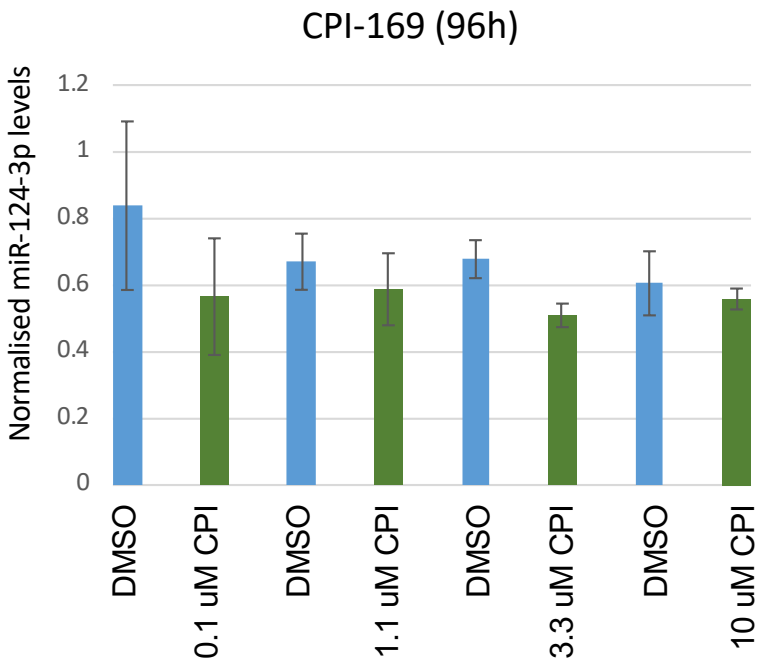
CPI-169 (96h)
Normalised miR-124-3p levels
1.2
1
0.8
0.6
0.4
0.2
0
DMSO
0.1 uM CPI
DMSO
1.1 uM CPI
DMSO
3.3 uM CPI
DMSO
10 uM CPI

Transparent Methods:

Cell culture

MCF7 cells (ATCC, HTB-22) and their derivatives were grown in DMEM Low Glucose (Gibco, 31885-023) supplemented with 10 % of FBS (Gibco, 10270-106), 40 µg/mL of gentamicin (Gibco, 15710-049) and 0.6 µg/mL of insulin (NovoRapid, 3525909). MDA-MB-231 cells (ATCC, HTB-26) and Cama-1 cells (ATCC, HTB-21) were grown in DMEM GlutaMAX (Gibco, 10566016) supplemented with 10 % of FBS (Gibco, 10270-106), 1 % penicillin/streptomycin (Gibco, 15140122). Cells were grown at 37°C and 5% CO_2 in a humidified incubator and passaged every 2 – 4 days by trypsinization. Sustained expression of ER-alpha in MCF7 and Cama-1 was validated regularly by western blotting and immunofluorescence. Cells were regularly tested for mycoplasma using a commercial kit (ATCC, 30-1012K), and cultures renewed from low passage stocks every two months or less.

Stable expression of CDYL2 in MCF7 and Cama-1 cells

CDYL2 cDNA was cloned by PCR from an MCF7 cDNA library using the primers in Table S3 and Phusion polymerase (NEB, M0530), and inserted into the Gateway pENTR-D-TOPO vector (Invitrogen, K240020). Sequencing on both strands confirmed that the cDNA corresponded to a published CDYL2 sequence (Genbank, NM_152342.2). The cloned cDNA was then transferred into MSCV plasmid (Addgene # 41033) using LR Clonase (Invitrogen, 11791100), and the resulting expression construct validated by sequencing. MCF7 or Cama-1 cells were then stably transduced with MSCV (Vector) or MSCV-CDYL2 retroviruses and selected for 14 days using 2 µg/mL puromycin (Sigma, P8833). Expression was confirmed by western blotting and immunofluorescence using CDYL2 antibody.

RNA interference and microRNA treatments

For transient RNAi, MDA-MB-231 cells were transfected with CDYL2 esiRNA (Sigma, EHU042511), esiLuciferase (Sigma, EHUFLUC), on-target plus p65 siRNA (Dharmacon, L-003533-00), or on-target plus STAT3 siRNA (Dharmacon, L-003544-00-0005) or on-target plus control siRNA (Dharmacon, D-001810-01-05) using Interferin reagent (Polyplus, 409-10)

according to the manufacturer's instructions. Cellular assays and analysis were performed between 48 and 72h post-transfection, according to the experiment. For stable RNAi, MCF7 cells were transduced with non-targeting control shRNA pLKO.1 lentiviruses (Sigma, SHC016) or shRNA-pLKO targeting CDYL2 (Sigma, shCDYL2 #1, TRCN0000359078; shCDYL2 #2, TRCN0000130741; shCDYL2 #3, TRCN0000129278), selected for 14 days using 2 μg/mL puromycin (Sigma, P8833). Cellular assays and analysis were then performed between weeks 2 and 4 post-transduction. The Hsa-miR-124-3p MISSION microRNA Mimic (Sigma, HMI0086) and or a Negative Control miRNA mimic (Sigma, HMC0002) were transfected into MCF7-Vector or MCF7-CDYL2 cells using Interferin reagent (Polyplus). Samples were harvested for analysis 48 – 72h post-transfection. The hsa-miR-124-3p Inhibitor (Qiagen, YI04102198-ADA), and its corresponding negative control (Qiagen, YI00199006-ADA) were co-transfected into MDA-MB-231 cells along with either esiCDYL2 or esiLuciferase siRNA, using Interferin reagent. Samples were harvested 72h later for analysis.

Antibodies and reagents

The following antibodies were used: CDYL2 (MyBiosource, MBS821304), ERα (Santa Cruz, sc-8002), β-Actin−HRP (Sigma, A3854), Vimentin (Dako, M0725), E-cadherin (BD 610682), Snail/Slug (Abcam, ab85936), Twist (Abcam, ab50887), Phospho-NF-κB p65 (Ser536) (Cell Signaling Technologies, #3031), total p65 (Cell Signaling Technologies, #3034), phosphor-STAT3 (Tyr705) (Cell Signaling Technologies, #9145), total STAT3 (Cell Signaling Technologies, #9139), CD44-FITC (Miltenyl Biotec, 130-113-341), CD24-PE (Miltenyl Biotec,130-095-953), APC anti-human CD326 (EpCAM) Antibody (Biolegend, 324208), PerCP/Cy5.5 anti-human/mouse CD49f Antibody (Biolegend, 313618), EZH2 (Cell Signaling Technologies #5246S), ChIP-grade EZH2 (Diagenode, C15410039), SUZ12 (Cell Signaling Technologies #3737S), H3K9me2 (Abcam, Ab1220), H3K27me3 (Diagenode, C15410069), rabbit IgG (Bethyl, P120-101), H3 (Abcam, Ab1791). The G9a and GLP antibodies were gifts from Y. Nakatani lab (Ogawa et al., 2002). UNC0642 and CPI-169 were obtained from Cayman Chemicals, re-suspended in cell-culture grade DMSO (Sigma), and used as described.

Immunoblot

Cells were washed with PBS, lysed in ice-cold RIPA buffer (10 mM Tris-Cl (pH 8.0), 1 mM EDTA, 1% Triton X-100, 0.1% sodium deoxycholate, 0.1% SDS, 140 mM NaCl, 1 mM PMSF, all from Sigma) containing protease inhibitor cocktail (Roche, 04693132001) phosphatase inhibitors cocktail (Roche, 4906845001), and sonicated briefly. Cleared lysates were boiled in Laemelli buffer, resolved on Bis-Tris NuPage Gels (Invitrogen), transferred to Nitrocellulose (GE Healthcare), and probed according to the primary antibody manufacturer's protocols. Images were collected using the ChemiDoc system (BioRad).

Co-Immunoprecipitation

Cells were grown to sub-confluence in 15 cm tissue culture treated plates (Corning). Monolayers were washed three times with ice-cold phosphate buffered saline (PBS), scraped in cold PBS containing a protease inhibitor cocktail (Roche) and pelleted. The resulting cell pellets were lysed in lysis buffer (50mM Tris pH8; 150mM NaCl; 1% NP-40; 2mM EDTA; all from Sigma) containing protease inhibitor cocktail (Roche, 04693132001) and phosphatase inhibitors cocktail (Roche, 4906845001). The lysates mechanically homogenized on ice using 25G syringes (BD, #300600), then incubated for 30 min at 4°C with rotation. Lysates were centrifuged at 12000 rpm for 15 min at 4°C. The resulting supernatants were treated with DNase I (Qiagen, #79254) and RNase A (Sigma, R4875), then precleared with protein A agaroses beads for 1 hour 4°C with rotation. Immunoprecipitation was performed by incubating indicated antibodies with the lysates overnight at 4°C with rotation, followed by addition of prewashed protein A agaroses beads for 2 hours 4°C with rotation. The beads were then washed 5 times with wash buffer (10mM Tris pH8; 1mM EDTA; 1mM EGTA; 250mM NaCl; 1% Triton) containing protease inhibitor cocktail (Roche, 04693132001) phosphatase inhibitors cocktail (Roche, 4906845001). The immune-precipitated beads were boiled in Laemmli buffer and then subjected to immunoblotting.

Immunofluorescence

Cells were seeded on sterilized coverslips. Forty-eight hours after seeding, cells were fixed with 4% fresh electron microscopy-grade paraformaldehyde (Fisher, 50-980-487) diluted in PBS (Sigma) for 15 minutes at room temperature. Fixed cells were permeabilized by NP-40 0.5% (Sigma) in PBS at room temperature for 15 minutes and blocked with 5% FBS in a PBS/0.1% NP-40 buffer, at room temperature for 1 hour. Coverslips were then probed with

the indicated primary antibodies 1h at room temperature and then Alexa dye tagged secondary antibody (see above) for 1 h at room temperature. Coverslips were mounted using DAPI mounting medium (Vectashield; Vector Laboratories) and observed under the upright microscope (Zeiss axioimager, SIP 60549), images were analyzed using Zen software (Zeiss).

Flow cytometry

The cells were labeled with anti-CD44-PerCP-Cy 5.5, anti-CD24-PE, APC anti-human CD326 (EpCAM) Antibody, PerCP/Cy5.5 anti-human/mouse CD49f Antibody, according to the manufacturer's instructions. All analyses were performed using a BD FACSCalibur flow cytometer and BD CellQuest software (BD Biosciences).

Gene expression

RNA was extracted using TRI-reagent (Sigma, T9424), and cDNA synthesized using the High-Capacity cDNA Reverse Transcription Kit (Applied Biosystems, #4368814). miRNA was extracted using the miRNeasy Mini Kit (Qiagen, #217004) following the manufacturer's instructions, and cDNA synthesized using miScript II RT Kit (Qiagen,#218161). The RT-qPCR was performed using the Fast SYBR Green 2X Master Mix (Applied Biosystems, #4385610) and an LC480 PCR machine (Roche). Primers are described in Table S3.

RNA-seq and enrichment analysis

RNA libraries were prepared with the TruSeq Stranded Total-RNA kit and sequenced on a Illumina NextSeq sequencing machine. After careful quality controls, raw data were aligned on the human genome (hg38) with STAR v2.7.0f (Dobin et al., 2013) and default parameters. Read counts on each genes of the Gencode annotation v29 were produced by STAR.

Unless otherwise specified, the analyses were performed using R (v 3.4.4) and illustrations produced with the ggplot2 (Wickham, H., 2016) and ggpubr packages. Starting from raw counts, we used the R package DESeq2 (Love et al, 2014) (v1.14) to perform the differential expression analyses. Each time the design was set as *~REP + TYPE,* where REP refers to the replicate number (paired analysis) and TYPE to the treatment group. Differential expression was tested using the Wald test, and p-values were corrected with the Benjamini-Hochberg method. To test the pathway enrichment of a list of genes, we used the R packages

clusterProfiler (Yu et al, 2012) (v 3.8.1), msgidbr (v 6.2.1), org.Hs.eg.db (v 3.5.0) and reactomePA (v 1.24) (Carlson, M, 2013). We tested the list of genes against pathways from msigdb hallmarks, GO molecular functions, KEGG and Reactome. Over-representation p-values were corrected with the Benjamini-Hochberg method.

Chromatin immunoprecipitation

For MDA-MB-231 ChIP-qPCR analysis, cells grown in 6-well plates were treated as described, then cross-linked by the addition of fresh 1% methanol-free formaldehyde to the cell culture medium for 10 minutes, followed by the addition of glycine to a final concentration of 125 mM for 5 minutes. Monolayers were washed three times with ice-cold PBS, scraped in cold PBS containing a protease inhibitor cocktail (Roche) and pelleted. Chromatin lysates were prepared from the cross-linked pellets, and ChIP assays performed using a commercial kit (Cell Signaling Technologies, #9003), with the indicated antibodies. Quantitative PCR was performed using the primers listed in Table S3. Input chromatin was purified in parallel in each ChIP assay and used to validate the chromatin digestion efficiency, and to determine the percentage of input recovered in each ChIP assay.

For MCF7 ChIP-seq and ChIP-qPCR analysis, cells were grown to sub-confluence in 15 cm tissue culture treated plates (Corning), cross-linked, washed and pelleted as described for MDA-MB-231 cells, above. The resulting cell pellets were pre-treated by incubating in lysis buffer A (Lysis Buffer 1 (50 mM HEPES pH 7.5; 140 mM NaCl, 1 mM EDTA, 10% glycerol, 0.5% NP-40, 0.25% Triton X-100, 1× protease inhibitors) for 10 minutes at 4°C, then lysis buffer B (10 mM Tris-HCl pH 8.0; 200 mM NaCl; 1 mM EDTA; 0.5 mM EGTA; 1× protease Inhibitors) for 10 minutes at room temperature, as previously described (Lee et al., 2006). They were then lysed in buffer C (10 mM Tris-HCl, pH 8.0, 100 mM NaCl, 1 mM EDTA, 0.5 mM EGTA, 0.1%; Na-Deoxycholate, 1× protease inhibitors) supplemented with 0.5% SDS, incubated on ice for 30 minutes with occasional vortexing, then sonicated on ice to an average fragment size of 150 bp using a sonicator (Branson, Digital Sonifier 450). The sonicated lysate was centrifuged at 12,000 r.p.m. in a benchtop centrifuge at 4°C, the supernatant diluted five times in buffer C, and 1 mL aliquots of this added to 50 µL of magnetic protein A beads (Invitrogen) pre-coated with 5 µg of anti-CDYL2 IgG. These were incubated overnight at 4°C with rotation, then pelleted and

washed with two sequential additions each of wash buffer 1 (0.1% SDS, 1%Triton X-100, 2mM EDTA, 20mM Tris-HCl, pH 8, 150mM NaCl), wash buffer 2 (0.1% SDS, 1%Triton X-100, 2mM EDTA, 20mM Tris-HCl, pH 8, 500mM NaCl), wash buffer 3 (0.25M LiCl, 1% NP40, 1% deoxycholate, 1mM EDTA, 10mM Tris-HCl, pH 8), and TE buffer (10mM Tris-HCl, 1mM EDTA, pH 8.0, 50 mM NaCl). Chromatin was eluted by incubating for 30 minutes at 65°C in elution buffer (50 mM Tris-HCl pH 8, 10 mM EDTA pH 8, 1% SDS) with frequent vortexing. Crosslinks were reversed by overnight incubation at 65°C, and eluates treated with RNAse A (Sigma) for 2h, followed by Proteinase K for 2h, then extracted using a classical Phenol-Chloroform/Ethanol precipitation protocol.

ChIP-seq

Pair end DNA sample libraries were sequenced using Illumina. Raw sequences were aligned to human genome hg19, using Bowtie 2.0 (Langmead and Salzberg, 2012) with paired-end parameters. Normalized and subtraction bigwig files were obtaining using deepTools (Ramírez et al., 2016). Analysis of ChIP-Seq data was in the galaxeast.fr instance. Significant peaks were called using MACS2 (Zhang et al., 2008, p. 2). Called peaks were annotated using Homer_AnnotatePeaks.

Colony formation assay

To form adherent colonies, 3000 cells were seeded in 12 well tissue-culture treated plates. After 14 days of growth, all colonies were stained with crystal violet solution (crystal violet 0.05%, formaldehyde 1%, methanol 1%) for 20min, washed extensively with water. Colonies were counted and their size was measured using *Fiji* software.

Migration and invasion assays

Real-time cell migration and invasion were measured using the *xCELLigence* RTCA DP apparatus (Acea Biosciences, Inc.) according to the manufacturer's protocol. Briefly, 40,000 cells were prepared in serum-deprived medium and then added to the upper chambers of *CIM-16 plates* (Aceabio, #5665817001). Complete medium containing 10% FBS was added to the lower chamber. For invasion assays, Matrigel diluted in serum-free medium at 500µg/mL (BD Biosciences, #354234) was added to the upper chamber and allowed to set before adding

cells. Migration across the membrane separating the two chambers was expressed as the Cell Index (CI).

Mammosphere formation assay

Cells were seeded at several densities (10, 50, 100, 1000 cells per well) in 96-well ultra-low attachment plates (Corning, #3474) with MEBM Basal Medium (Lonza, CC-3151) containing 2% B-27 (Invitrogen, 17504-044), 20 ng/mL EGF (Sigma, E9644), 4 µg/mL insulin (Novo Nordisk, # 3525909), and 2 µg/mL hydrocortisone (Sigma, H0135). Mammospheres were cultured for 1-2 weeks, with image collection approximately every three days starting at day 8. Whole-well images were taken with the *IncuCyte ZOOM* System (Essen Bioscience) using a 4X phase contrast objective. Mammosphere diameter and the number of mammospheres >50µm were determined by image analysis using Fiji software (Fiji).

Zebrafish embryo metastasis assay

Zebrafish embryos were raised under standard experimental conditions. Cells trypsinated, resuspended in serum-free media, and stained with lipophilic dyes DiO or DiD from the Vybrant Multicolor Cell-Labeling Kit (Invitrogen, V22889) for 20 minutes at 37°C, then washed resuspended in PBS 1x. 48 hours post-fecundation, the embryos were dechorionated and anesthetized with tricaine (Sigma-Aldrich, E10521). The anesthetized embryos were subjected to microinjection. 20nl of cell suspension, which represent approximately 300 labeled human cells, were injected into perivitelline space of each embryo. The injected zebrafish embryos were immediately placed at 30°C for 24 hours in presence of N-phenylthiourea (Sigma-Aldrich, P7629) to inhibit melanocyte formation. For metastasis assessment, The anesthetized embryos were evaluated using the fluorescent microscope Axio Observer Zeiss microscope (Zeiss).

Statistical analysis

CDYL2 expression levels from *TCGA* were stratified based on molecular markers such as ERα and HER2 expression by IHC. Correlation analysis between CDYL2 RNA and protein levels were performed using *GraphPad Prism7*. For overall survival analysis, patients were divided into

two groups (low and high CDYL2) using the expression level of CDYL2 and best cutoff. Kaplan-Meier survival plots, log-rank p-values, hazard ratios were calculated using GraphPad Prism7.

Supplemental References:

Carlson, M, 2013. Genome wide annotation for Human. R package version, 3(1).

Dobin, A., Davis, C.A., Schlesinger, F., Drenkow, J., Zaleski, C., Jha, S., Batut, P., Chaisson, M., Gingeras, T.R., 2013. STAR: ultrafast universal RNA-seq aligner. Bioinformatics 29, 15–21. https://doi.org/10.1093/bioinformatics/bts635

Langmead, B., Salzberg, S.L., 2012. Fast gapped-read alignment with Bowtie 2. Nat. Methods 9, 357–359. https://doi.org/10.1038/nmeth.1923

Ogawa, H., Ishiguro, K., Gaubatz, S., Livingston, D.M., Nakatani, Y., 2002. A complex with chromatin modifiers that occupies E2F- and Myc-responsive genes in G0 cells. Science 296, 1132–6.

Ramírez, F., Ryan, D.P., Grüning, B., Bhardwaj, V., Kilpert, F., Richter, A.S., Heyne, S., Dündar, F., Manke, T., 2016. deepTools2: a next generation web server for deep-sequencing data analysis. Nucleic Acids Res. 44, W160-165. https://doi.org/10.1093/nar/gkw257

Wickham, H., 2016. ggplot2: Elegant Graphics for Data Analysis.

Zhang, Y., Liu, T., Meyer, C.A., Eeckhoute, J., Johnson, D.S., Bernstein, B.E., Nusbaum, C., Myers, R.M., Brown, M., Li, W., Liu, X.S., 2008. Model-based analysis of ChIP-Seq (MACS). Genome Biol. 9, R137. https://doi.org/10.1186/gb-2008-9-9-r137